The Structure of a Peptide-Loaded Shark MHC Class I Molecule Reveals Features of the Binding between β_2-Microglobulin and H Chain Conserved in Evolution

Yanan Wu,*[,1] Nianzhi Zhang,*[,1] Xiaohui Wei,* Shuangshuang Lu,* Shen Li,* Keiichiro Hashimoto,[†] Johannes M. Dijkstra,[†] and Chun Xia*

Cartilaginous fish are the most primitive extant species with MHC molecules. Using the nurse shark, the current study is, to the best of our knowledge, the first to present a peptide-loaded MHC class I (pMHC-I) structure for this class of animals. The overall structure was found to be similar between cartilaginous fish and bony animals, showing remarkable conservation of interactions between the three pMHC-I components H chain, β_2-microglobulin (β_2-m), and peptide ligand. In most previous studies, relatively little attention was given to the details of binding between the H chain and β_2-m, and our study provides important new insights. A pronounced conserved feature involves the insertion of a large β_2-m F56+W60 hydrophobic knob into a pleat of the β-sheet floor of the H chain α1α2 domain, with the knob being surrounded by conserved residues. Another conserved feature is a hydrogen bond between β_2-m Y10 and a proline in the α3 domain of the H chain. By alanine substitution analysis, we found that the conserved β_2-m residues Y10, D53, F56, and W60—each binding the H chain—are required for stable pMHC-I complex formation. For the β_2-m residues Y10 and F56, such observations have not been reported before. The combined data indicate that for stable pMHC-I complex formation β_2-m should not only bind the α1α2 domain but also the α3 domain. Knowing the conserved structural features of pMHC-I should be helpful for future elucidations of the mechanisms of pMHC-I complex formation and peptide editing. ***The Journal of Immunology*****, 2021, 207: 308–321.**

Cartilaginous fish (Chondrichthyes; sharks, rays, and chimeras) and bony animals (Osteichthyes; bony fish and tetrapods) separated ∼450 million years ago, and together they comprise all extant jawed vertebrates (Gnathostomata) (1). Their adaptive immune systems are similar, whereas they are different from immune defenses in jawless fish (Agnatha; hagfish and lampreys) and invertebrates (2–7). Similar to other jawed vertebrates, sharks have B cells and T cells that express cell surface receptors of the Ig superfamily (IgSF) from somatically rearranged genes in a clonal fashion. For B cells, these receptors comprise different classes of Abs, including IgM (2). The individual TCR chains comprise, besides some noncanonical assemblies, the chains TCRα, -β, -γ, and -δ (2, 6). Furthermore, as in mammals, sharks have a thymus for T cell education. The biggest differences from the mammalian immune system, arguably, are the absence of lymph nodes and the fact that sharks are ectotherms.

TCRαβ T cells only recognize peptide Ags if presented by MHC molecules (8, 9). In the early 1990s, we were the first to report MHC class I and II (MHC-I and MHC-II) genes in bony fish (10) as well as a partial MHC gene in sharks (11). Soon after, this was followed by the identification of polymorphic shark MHC-IIα and MHC-IIβ genes by others (12–14), after which we were the first to determine shark MHC-I allelic polymorphism (15). High allelic polymorphism in shark MHC-I and MHC-II was found to be similar, as in mammals, with many of the highly polymorphic residues predicted to line the peptide-binding grooves (13–16).

In jawless fish and invertebrates, MHC genes or homologs thereof have not been found, and cartilaginous fish are the most primitive extant species with MHC genes (2, 7). An apparently primitive feature in sharks is that the genes for MHC-I, MHC-IIα, MHC-IIβ, and β_2-microglobulin (β_2-m), which are related and whose origin presumably involved tandem gene duplications, are still linked in the genome (17, 18). Except for some bony fishes (19–21), probably all investigated jawed vertebrate species possess polymorphic MHC-I and MHC-II molecules that are known or expected to present peptide Ags to TCRαβ T cells. These MHC molecules are called "classical." However, at various times during jawed vertebrate evolution, duplications of classical MHC-I and MHC-II genes generated "nonclassical" MHC variants with a diversity of functions that are not shared throughout jawed vertebrates (22–27). In the present study, unless indicated differently, MHC-I and MHC-II refer to the classical molecules. The evolutionary origin of MHC molecules, before the establishment of classical MHC-I, MHC-IIα, MHC-IIβ, and β_2-m, is not known.

*Department of Microbiology and Immunology, College of Veterinary Medicine, China Agricultural University, Beijing, China; and [†]Institute for Comprehensive Medical Science, Fujita Health University, Toyoake, Japan

[1]Y.W. and N.Z. contributed equally to this work.

ORCIDs: 0000-0003-4964-888X (Y.W.); 0000-0001-6660-0242 (X.W.); 0000-0001-8643-9994 (S.L.); 0000-0001-7097-3826 (J.M.D.); 0000-0002-3444-0624 (C.X.).

Received for publication October 16, 2020. Accepted for publication April 23, 2021.

This work was supported by the National Basic Research Program of China (973 Program) (Grant 2013CB835302), the Japan Society for the Promotion of Science Grants-in-Aid for Scientific Research (Grant JP26440201), and the National Natural Science Foundation of China.

The coordinates and structure factors presented in this article have been submitted to the Protein Data Bank (https://www.rcsb.org/) under accession numbers 6LUP and 6LUO.

Address correspondence and reprint requests to Dr. Johannes M. Dijkstra or Prof. Chun Xia, Institute for Comprehensive Medical Science, Fujita Health University, Toyoake 470-1192, Japan (J.M.D.) or Department of Microbiology and Immunology, College of Veterinary Medicine, China Agricultural University, Beijing 100193 (C.X.). E-mail addresses: dijkstra@fujita-hu.ac.jp (J.M.D.) or xiachun@cau.edu.cn (C.X.)

Abbreviations used in this article: HC, H chain; IgSF, Ig superfamily; β_2-m, β_2-microglobulin; MHC-I, MHC class I; MHC-II, MHC class II; pMHC-I, peptide-loaded MHC class I; PDB, Protein Data Bank; TAPBP, TAP binding protein; TAPBPR, TAPBP-related.

Previously, based on conservation of MHC-I H chain (HC) residues, we predicted that shark HC binds its smaller partner β_2-m and the termini of the peptide ligand by similar interactions as in mammals (15, 16). Similarity in the HC-to-β_2-m binding mode was also suggested after analysis of cartilaginous fish β_2-m sequences (28, 29). However, hitherto, there have not been studies on shark MHC molecules at the protein level except for our analysis of a free (not bound to HC) β_2-m structure (30). To our knowledge, the present study is the first to determine the peptide binding preferences of a shark MHC-I allele and, by using X-ray crystallography, the structure of shark pMHC-I. We also present a detailed structural analysis of the HC-to-β_2-m binding mode, as done for pHLA-A2 in the seminal paper by Saper et al. in 1991 (31), revealing conservation of critical binding features throughout jawed vertebrates. Furthermore, based on mutation analysis, the current study is, to our knowledge, the first to show the importance of β_2-m residues Y10 and F56 for pMHC-I complex formation. Whereas the importance of β_2-m with HC-α1α2 domain interaction was already known (32, 33), the observed importance of β_2-m Y10 suggests that also the binding of β_2-m to the HC-α3 domain is critical for pMHC-I complex formation.

Materials and Methods

Production, crystallization, and structural determination of recombinant nurse shark pUAA and free β_2-m

Preparation of proteins. DNA fragments encoding the ectodomain of nurse shark (*Ginglymostoma cirratum*) classical MHC-I allele Gici-UAA*01 (17), represented by residues 17–283 of GenBank accession https://www.ncbi.nlm.nih.gov/nuccore/AF220063, and mature Gici-β_2-m (18), represented by residues 18–111 of GenBank accession https://www.ncbi.nlm.nih.gov/nuccore/HM625831 with termini slightly modified as described in (30), plus an appropriate stop codon and flanking NdeI and XhoI restriction sites, were synthesized by Shanghai Invitrogen Life Technologies, cloned after NdeI/XhoI digestion into pET21a(+) vectors (Novagen) and expressed in *Escherichia coli* strain BL21 (DE3). Recombinant Gici-UAA*01 and Gici-β_2-m were expressed as inclusion bodies and purified as described previously (34). The Gici-UAA*01 and Gici-β_2-m inclusion bodies were separately dissolved in 6 M guanidinium chloride buffer to a protein concentration of 30 mg/ml.

Preparation of the nurse shark β_2-m mutants Y10A, D53A, F56A, and W60A. In the above-described recombinant *Gici-β_2-m* sequence the codons for Y10, D53, F56, and W60 were individually mutated to alanine codons by overlap PCR. Primers used were as follows: for Y10A, 5′-TGCAGGTGGCGACCTATAAA-3’ and 5′-TTTATAGGTCGCCACCTGCA-3′; for D53A, 5′-ACCCAGAGCGCGCTGAGCTTT-3′ and 5′-AAAGCTCAGCGCGCTCTGGGT-3′; for F56A, 5′-GATCTGAGCGCGGAAAGCGATT-3′ and 5′-AATCGCTTTCCGCGCTCAGATC-3′; for W60A, 5′-GAAAGCGATGCGAGCTTCAAAC-3′ and 5′-GTTTGAAGCTCGCATCGCTTTC-3′. These mutants were expressed as inclusion bodies and purified as described above.

Peptide synthesis. Binding affinities of nonamer peptides were predicted using the NetMHCpan 2.8 server (http://www.cbs.dtu.dk/services/NetMHCpan/) (35). Nonamer peptides used in the experiments (Supplemental 1A) were synthesized and purified to 90% by reverse-phase HPLC and mass spectrometry (SciLight Biotechnology). The peptides were stored in lyophilized aliquots at −80°C after synthesis and were dissolved in DMSO before use. For the Ran_9X$_{splitted}$ synthetic random nonapeptide library, see Qu et al. (36).

Assembly of pGici-UAA complexes. To assemble pGici-UAA complexes, the Gici-UAA*01 and Gici-β_2-m inclusion bodies and the respective peptide (in a 1:1:3 molar ratio) were refolded according to the gradual dilution method that we described previously (37). After 24-h refolding at 277 K and spinning out aggregates, the protein preparation was concentrated and purified using a Superdex 200 16/60 column (GE Healthcare), followed by Resource Q anion-exchange chromatography (GE Healthcare). The eluted peaks were collected and tested by SDS-PAGE (38). The purified proteins were buffer exchanged into 20 mM Tris-HCl (pH 8.0), 50 mM NaCl three times using Amicon Ultra-15 centrifugal filter devices (Millipore) with a molecular mass cutoff of 10,000 kDa and concentrated.

Refolding of free nurse shark β_2-m. Soluble Gici-β_2-m protein was prepared with refolding assays as described previously with modifications in our laboratory (30, 34). After 12 h of refolding at 277 K and spinning out aggregates, the protein preparation was concentrated, purified, and then buffer exchanged as described for pGici-UAA.

Crystallization and data collection

pGici-UAA complex. The purified pGici-UAA complex consisting of Gici-UAA*01, Gici-β_2-m, and peptide pep56 (FANFFIRGL) was diluted to 10 mg/ml. After mixing with reservoir buffer at a 1:1 ratio, the purified protein was crystallized by the hanging-drop vapor diffusion technique at 291 and 277 K. Index, Crystal Screen I/II, and Crystal Screen Cryo I/II kits (Hampton Research, Riverside, CA) were used to screen for optimal crystal growth conditions. After several days, crystals of the pGici-UAA complex were observed with solution NO.38 from the Crystal Screen Cryo I kit (pH 7.5, 0.09 M HEPES sodium, 1.26 M sodium citrate tribasic dihydrate, and 10% [v/v] glycerol) at 277 K. The crystals were first soaked in reservoir solution containing 25% glycerol as a cryoprotectant and were then flash-cooled in a stream of gaseous nitrogen at 100 K (39). Diffraction data of pGici-UAA crystals were collected to a resolution of 2.3 Å using beam line BL17U of the Shanghai Synchrotron Radiation Facility (Shanghai, China). The collected intensities were indexed, integrated, corrected for absorption, scaled, and merged using the HKL2000 package (40).

Free nurse shark β_2-m. Purified Gici-β_2-m was diluted to 7 mg/ml and then crystallized as described for pUAA. After several days, crystals suitable for data collection were obtained in solution NO.39 from the Crystal Screen I kit (0.1 M HEPES sodium [pH 7.5], 2% [v/v] polyethylene glycol 400, 2.0 M ammonium sulfate) at 291 K. Prior to data collection, the crystals were soaked in reservoir solution supplemented with 15% (v/v) glycerol as a cryoprotectant several seconds and flash-cooled in a stream of gaseous nitrogen at 100 K or directly in liquid nitrogen at 77 K (30). The diffraction data of Gici-β_2-m crystals were collected on beamline NE3A at the High Energy Accelerator Research Organization (KEK) synchrotron facility (Tsukuba, Japan) at a wavelength of 1.0 Å using an ADSC Q270 imaging-plate detector. The collected data were indexed, integrated, corrected for absorption, scaled, and merged as described for pGici-UAA.

Analysis of stably bound peptides from a random mix of 9-aa peptides

For analysis of peptides that were stably bound by Gici-UAA*01 from a mix of random 9-aa peptides, a method was used that we described previously (36). In short, a Ran_9X$_{splitted}$ (XXXXXXXXX, where X is a random amino acid other than cysteine) synthetic random nonapeptide library was renatured with β_2-m and HC using the diluted renaturation method. After purification through gel filtration and anion exchange chromatography, the purified pMHC-I complex solution was concentrated, and the bound peptides were eluted with 0.2 N acetic acid and concentrated using a 3-kDa filter. Then, the eluted peptides were sampled for liquid chromatography-tandem mass spectrometry and de novo analysis. Finally, a sequence logo figure (https://weblogo.berkeley.edu/logo.cgi/logo.cgi) was shown of the amino acid distribution at positions 1–9.

Structure determination and refinement

*Nurse shark pUAA (Gici-UAA*01/Gici-β_2-m/pep56).* The crystal of shark pUAA belongs to the P64 space group with unit cell constants a = 125.86 Å, b = 125.86 Å, c = 132.47 Å, a = b = 90.00°, and c = 120.00° (see Supplemental 1B). The structure was solved by molecular replacement using Molrep and Phaser in the CCP4 package, with grass carp (*Ctenopharyngodon idella*) pMHC-I (“carp pUAA”; Protein Data Bank [PDB] code 5Y91) (41) as the search model (42–44). Extensive model building was performed by hand with Coot (45), and restrained refinement was performed using REFMAC5. Additional rounds of refinement were performed using the PHENIX refinement program implemented in the PHENIX package (46), along with isotropic atomic displacement parameter refinement and bulk solvent modeling. The stereochemical quality of the final model was assessed with the PROCHECK program (47).

Free nurse shark β_2-m. The structure of Gici-β_2-m was solved, refined, and stereochemical quality was assessed as described for pGici-UAA, using grass carp β_2-m (PDB code: 3GBL) as the search model. Detailed statistics for data collections and refinements are listed in Supplemental 1B.

Alignment of MHC sequences

The sequence alignment between various MHC-I and MHC-II sequences was made with the intention to align, as well as possible, evolutionarily corresponding residues. Representative MHC sequences were aligned by hand (16, 24–26) based on similarities between sequences, considerations of likely evolutionary events, and structural comparisons of various pMHC-I and pMHC-II (Supplemental 2). For most parts of the β-strands and helices, the alignments are unambiguous, but in many of the loop regions, and in some β-strand and helical regions with insertions or deletions, the best possible alignment is uncertain. That superimposition of structures does not provide definite clues for all parts of the alignment can be seen in Supplemental 2C.

Secondary structures as indicated in the sequence alignment figures were determined by DSSP software (https://swift.cmbi.umcn.nl/gv/dssp/) (48).

Calculations and generation of illustrations

Peptide-contacting residues were identified using the program CONTACT and were defined as residues containing an atom within 4.0 Å of the target partner (43). Structural illustrations and the electron density-related figures were generated using the PyMOL molecular graphics system (http://www.pymol.org/), and the same software system was used for making structural superposition figures by using the program "super" and to calculate dihedral angles of the pep56 backbone using the program "Measurement - Dihedrals". PDBePISA software (http://www.ebi.ac.uk/msd-srv/prot_int/cgi-bin/piserver) (49) was used for interdomain contact analysis and for measuring the exposed surface areas (= accessible surface area minus buried surface area) of the peptide ligands. The PDB accessions of the pMHC-I structures shown as representative structures are: Carp UAA, grass carp (*C. idella*) UAA, 5Y91; frog UAA, African clawed frog (*Xenopus laevis*) UAAg, 6A2B; chicken (*Gallus gallus*) BF2*0401, 4E0R; HLA-A2, 3PWN; mouse (*Mus musculus*) H2-Ag7, 1F3J; HLA-DR1, 1AQD. For comparisons of a large number of pMHC-Is, structures with the following PDB accession numbers were analyzed: HLA-A*0101 (4NQV), HLA-A*0201 (3PWN), HLA-A*0203 (3OX8), HLA-A*0206 (3OXR), HLA-A* A0207 (3OXS), HLA-A* 0301 (3RL1), HLA-A*1101 (1X7Q), HLA-A*2402 (2BCK), HLA-A*6801 (4HX1), HLA-A*6802 (4HWZ), HLA-B*0701 (3VCL), HLA-B*0801 (1M05), HLA-B*1402 (3BVN), HLA-B*1501 (1XR8), HLA-B*1801 (4JQV), HLA-B*2705 (1HSA), HLA-B*2709 (1UXW), HLA-B*3501 (1A9E), HLA-B*3505 (4JRX), HLA-B*3508 (3VFR), HLA-B*3901 (4O2C), HLA-B*4103 (3LN4), HLA-B*4402 (1M6O), HLA-B*4403 (1N2R), HLA-B*4405 (1SYV), HLA-B*4601 (4LCY), HLA-B*5101 (1E27), HLA-B*5201 (3W39), HLA-B*5301 (1A1O), HLA-B*5701 (2RFX), HLA-B*5703 (2BVO), HLA-C*0801 (4NT6), HLA-C*CW3 (1EFX), HLA-C*CW4 (1IM9), H-2*Db (1WBX), H-2*Dd (3E6H), H-2*Kb (3TID), H-2*Kd (1VGK), H-2*Kk (1ZT1), H-2*Kw_M7 (3FOL), H-2*Ld (1LD9), RT1-Aa (1ED3), RT1-Ac (1KJV), Mamu-A1 (1ZVS), Mamu-B17 (3RWC), SLA-1*0401 (3QQ3), BoLA-N*1801 (3PWU), BF2*0401 (4E0R), BF2*2101 (3BEV), Xela-UAA (6A2B), Ctid-UAA (5Y91), Gici-UAA (6LUP).

Protein structure accession numbers

The coordinates and structure factors for the Gici-UAA*01/Gici-β_2-m/FANFFIRGL complex and for free Gici-β_2-m have been deposited in the PDB under accession numbers 6LUP (http://www.rcsb.org/structure/6LUP) and 6LUO (http://www.rcsb.org/structure/6LUO), respectively.

Results

Formation of stable shark pMHC-I complexes consisting of HC, β_2-m, and a compatible nonamer peptide

Stable nurse shark pMHC-I complexes, as known for pMHC-I of other species, were formed as heterotrimers of HC (Gici-UAA*01), β_2-m, and a nonamer peptide with compatible sequence features, as revealed by chromatography after in vitro refolding (Fig. 1A, 1B; Supplemental 1A). Peptide ligand alanine substitution analysis, based on the sequence of stably binding peptide pep56 (FANFFIRGL) (Supplemental 1A), showed selective requirements at peptide positions P3, P5, P6, and P9 for forming stable pMHC-I (Fig. 1A, 1B). Mass spectrometry analysis of peptides that, in vitro, from a random mix of 9-aa

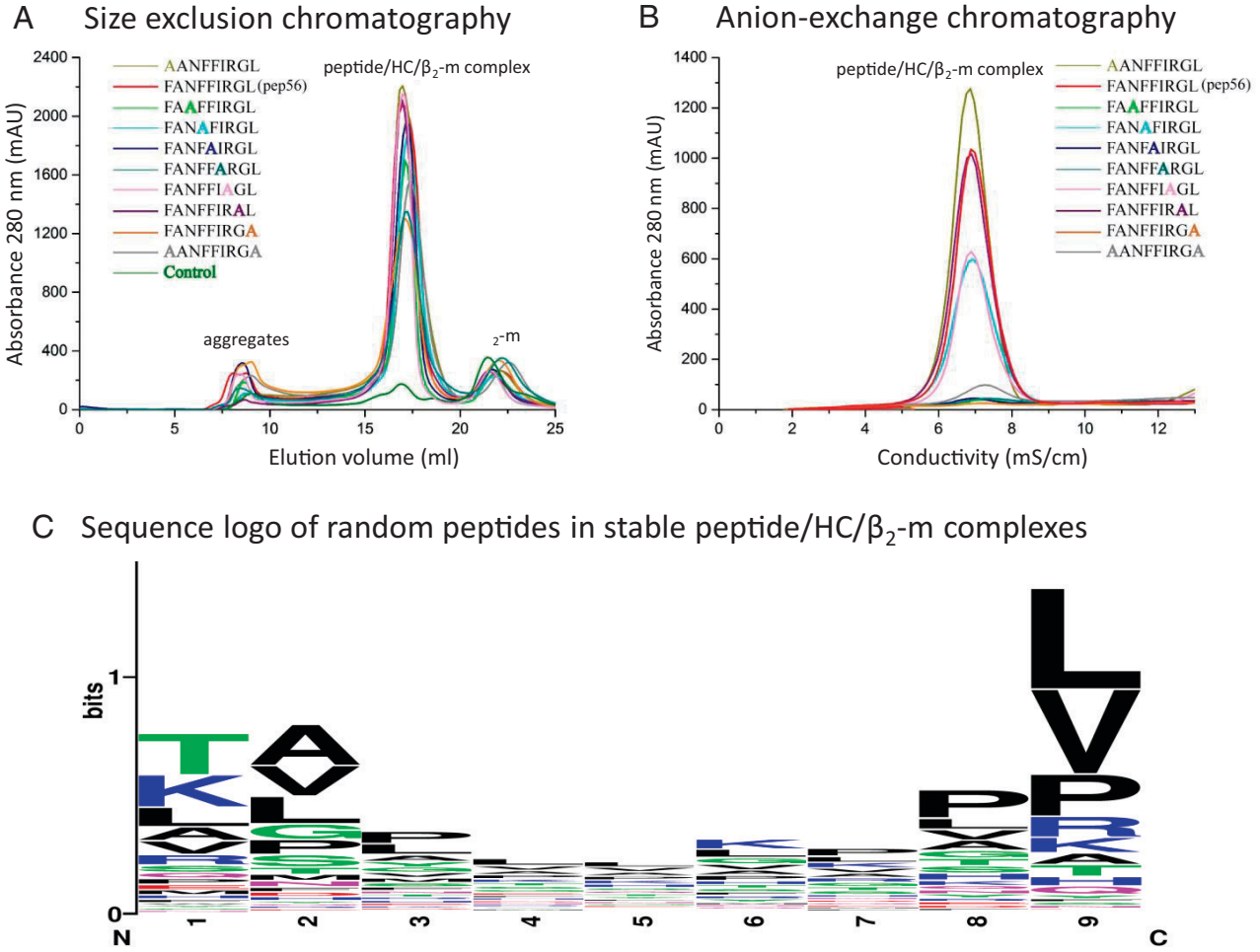

FIGURE 1. Peptide-sequence dependency of shark pMHC-I complex building. (**A**) Formation of pMHC-I complexes consisting of shark Gici-UAA*01, β_2-m, and either pep56 nonamer peptide, an alanine-substituted pep56-derived nonamer, or no peptide (control) was assayed by size exclusion chromatography (gel filtration). (**B**) The stability of the isolated pMHC-I complexes was subsequently analyzed by anion exchange chromatography. (**C**) In another experiment, random nonamer peptides were incubated with Gici-UAA*01 and β_2-m, and the sequences of the peptides that remained stably bound in pMHC-I complexes were analyzed by mass spectrometry and their sequence logo was determined.

peptides were stably integrated into pMHC-I complexes revealed selection at peptide position P9 (preferred residues were L or V) and, to a lesser extent, at position P2 (preferred residues were A, V, or L) (Fig. 1C). The combined results suggest that at especially position P9 the peptide ligand residue is being selected for, whereas selection at some other positions may depend on the within-peptide context.

*The overall structure of pep56/Gici-UAA*01/β_2-m (shark pUAA) is similar to pMHC-I of other species*

By X-ray crystallography, the structure of the pep56/Gici-UAA*01/β_2-m complex was determined at a resolution of 2.3 Å (Supplemental 1B) and is referred to in the current study as "shark pUAA." Similar to pMHC-Is of other species, shark pUAA α1 and α2 domains together build a pseudo-symmetric structure, forming a closed groove that consists of two anti-parallel right-handed helical structures on top of a β-sheet in which a peptide ligand is bound (Fig. 2A). The α3 and β_2-m domains form IgSF domain structures of the C1 category and each contains two antiparallel β-pleated sheets (50–52). Notable is the asymmetric organization of the α3 domain versus the β_2-m domain relative to the α1α2 domain (also known as the peptide binding domain) (Fig. 2A), as known for other pMHC-Is (51).

With the elucidation of shark pUAA, pMHC-I structures are now known for a variety of placental mammals (36, 51, 53), including chickens and ducks (54–56), the amphibian African clawed frog (57), the bony fish grass carp (41, 58), and the nurse shark (Fig. 2Ba). Superposition of representative pMHC-I structures reveals the overall similarity of shark pUAA with pMHC-Is of bony animals (Fig. 2Bb) and indicates that this type of structure was established more than 450 million years ago (Fig. 2Ba) (1). The biggest difference among pMHC-I structures concerns the orientation of the α3 domain (Fig. 2Bb), as observed previously (41, 54), and this is also the domain with the most internal variation (Supplemental 1C, 2Bb).

Sequence comparisons

Shark MHC-I sequences are compared with other representative MHC-I and MHC-II molecules for which the structures are known in Supplemental 2A with underlining and numbering of β-strand and helical structures. A larger set of representative MHC sequences are aligned in Supplemental 2B. Interesting conservation patterns are highlighted by color shading and help to recognize the residues that are specific for MHC-I. Residue numbering throughout this study follows the numbering for human HLA-A2 and β_2-m as done by Saper et al. (31).

Groove pockets and orientation of the peptide ligand in shark pUAA

Fig. 3A–D shows the orientation of pep56 within the elucidated shark pUAA structure, and its backbone ϕ and ψ torsion angles are listed in Fig. 3E. As commonly found for peptide ligands in other pMHC-Is, the side chains of the pep56 N-terminal and C-terminal residues (P1 and P9) are in upward and downward orientation, respectively (Fig. 3A). The pep56 backbone conformation follows a main theme found for peptide ligands in most, although not all, pMHC-Is (59). That is to say, the N-terminal four residues (P1–P4) and the C-terminal three residues (P7–P9 in case of shark pUAA) form extended left-handed helix type conformations, reminiscent of poly-L-proline type II helices (60), whereas the orientation of the middle region (P5–P6 in case of shark pUAA) shows extensive variation between pMHC-Is (e.g., 61, 62). In shark pUAA, as common among pMHC-Is (59, 63), the P4–P8 stretch is elevated (Fig. 3A, 3B) and provides the bulk of the exposed peptide surface area (Fig. 3D). In shark pUAA, the pep56 conformation appears to be stabilized by two sets of intramolecular interactions, namely, by polar contacts between the P3-N side chain carbonyl group and the P4-F and P5-F main chain amino groups, and by contact between the P4-F and P5-F aromatic rings (Fig. 3F).

In Fig. 3C, the "pocket" regions A–F are indicated for shark pUAA, based on the locations of those pockets in pHLA-A2 (31, 62),

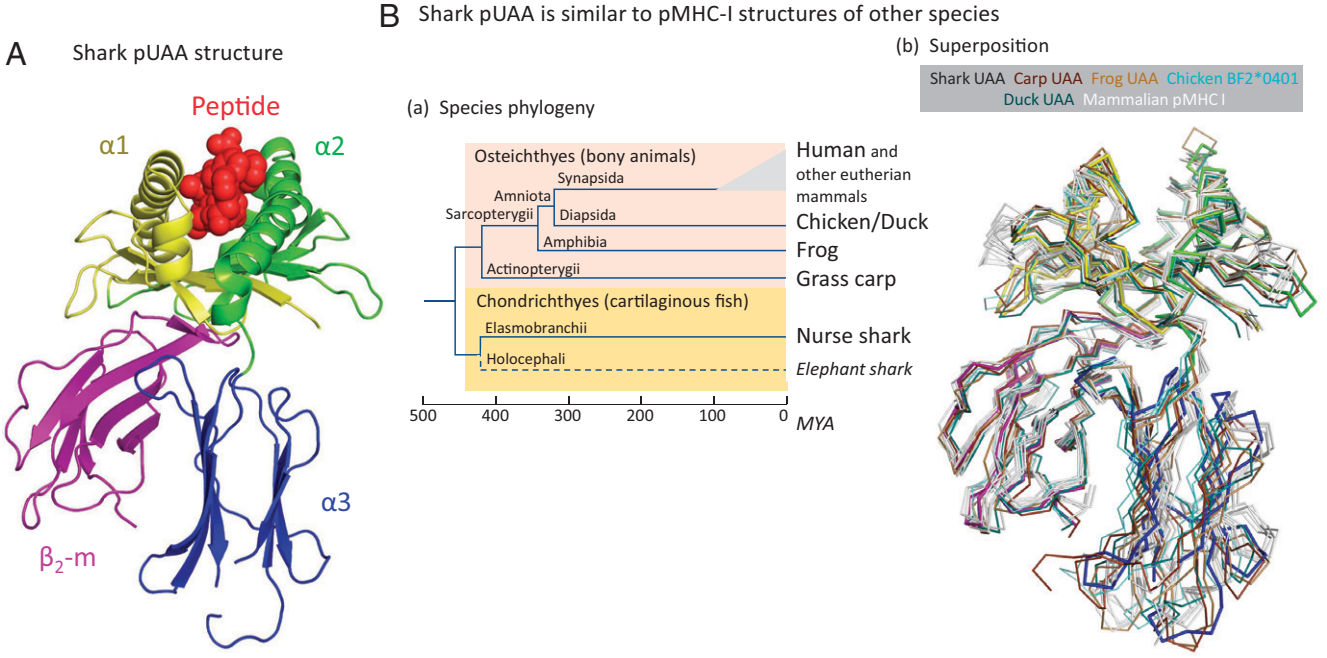

FIGURE 2. The overall structure of nurse shark pep56/Gici-UAA*01/β_2-m (shark pUAA) is similar to pMHC-I structures of other species. (**A**) Shark pUAA structure with HC and β_2-m depicted in a cartoon format and pep56 in a spheres format. (**Ba**) Phylogeny (1) of species for which pMHC-I structures have been determined plus elephant shark. The timescale is in millions of years ago (MYA). Elephant shark was only added to the tree to help estimate the age of residues specific to MHC-I in cartilaginous fish (see Supplemental 2B). (**Bb**) Superposition of representative pMHC-I structures shown without their peptide ligands and with the shark pUAA domains colored as in (A). For PDB accession numbers, see *Materials and Methods*.

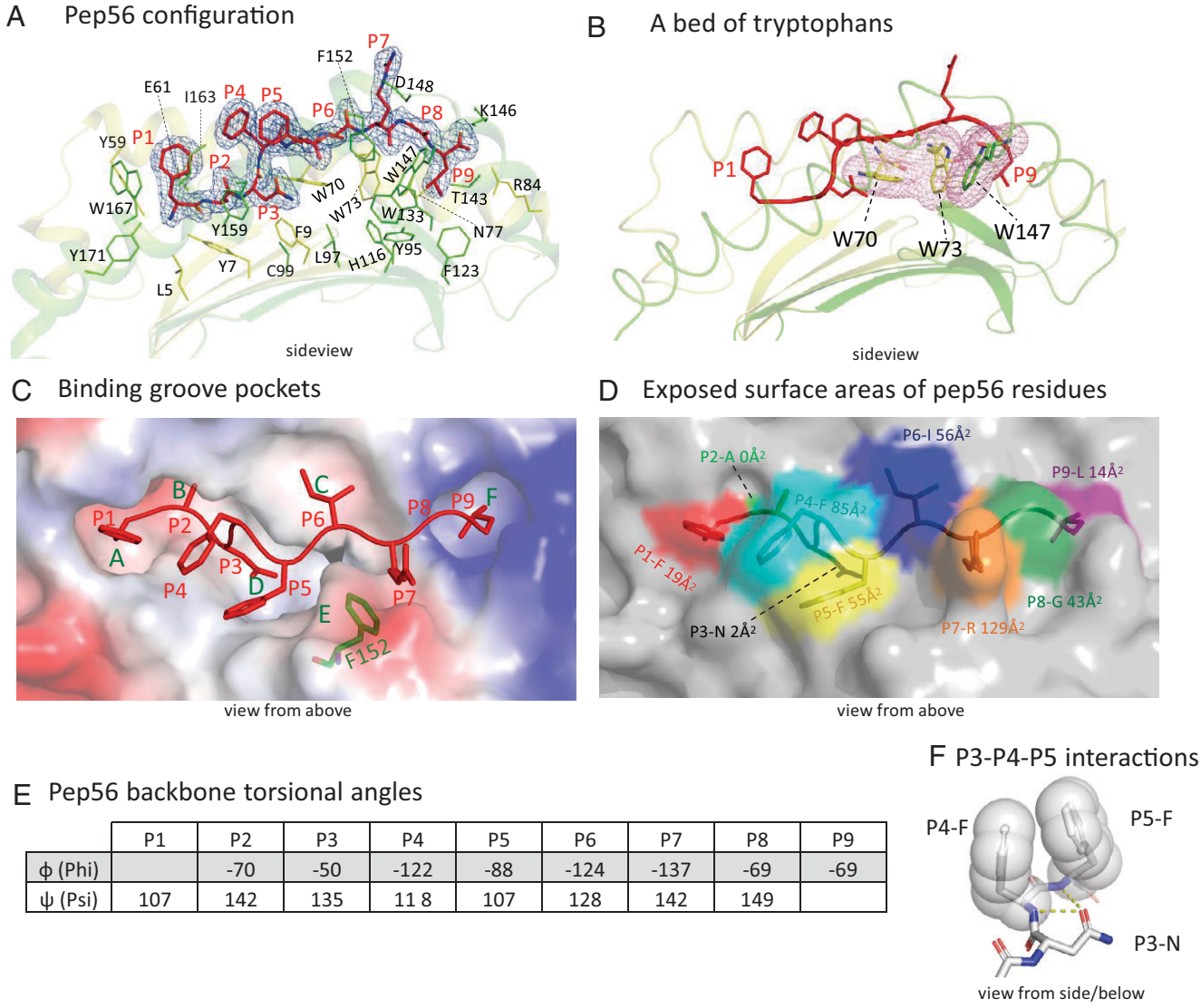

	P1	P2	P3	P4	P5	P6	P7	P8	P9
ϕ (Phi)		-70	-50	-122	-88	-124	-137	-69	-69
ψ (Psi)	107	142	135	11 8	107	128	142	149	

FIGURE 3. Peptide pep56 (FANFFIRGL) configuration in shark pUAA. (**A**) Side view of pep56 (red) in the shark pUAA peptide binding groove; side chains of groove α1 (yellow) and α2 (green) residues are highlighted in a sticks format. (**B**) This figure highlights the space occupied by the tryptophans W70, W73, and W147. (**C**) Shark pUAA shown from above with pep56 in a red cartoon/sticks format and HC in a transparent surface format with colors indicating electrostatic potential; F152 is additionally shown in a sticks format with green for C atoms. (**D**) Shark pUAA shown from above in a transparent surface format with unique colors for the pep56 residues, which are also shown in a cartoon/sticks format; surface areas contributed by the individual pep56 residues are indicated in $Å^2$. (**E**) Φ and Ψ torsional angles of pep56 in shark pUAA. (**F**) Stretch of pep56 shown in a sticks format with side chains of P4-F and P5-F additionally shown in a transparent spheres format. Stacked ring-type contact between P4-F and P5-F, and polar contacts between the P3-N side chain carbonyl group and the P4-F and P5-F main chain amino groups, may stabilize pep56 configuration.

as commonly done in pMHC-I literature (54). However, in contrast to many other pMHC-Is, shark pUAA does not have an E pocket accessible for accommodation of a P7 side chain, and the pep56 P7 side chain rotates upward (Fig. 3A–D). The absence of an accessible E pocket can be explained by a large phenylalanine in the α2 domain helix (F152) that points into the groove (Fig. 3C).

The C-terminal end of the peptide ligand in shark pUAA is elevated higher than commonly found among pMHC-Is and lays on a ridge consisting of the bulky residues W73 and W147 (Fig. 3B), with only the latter conserved among MHC-I sequences (Supplemental 2Ba). Fig. 3B also highlights tryptophan W70, as it makes for a shallow hydrophobic C pocket that binds P6-I. The shark pUAA residues W70, W73, and F152 are not conserved among reported nurse shark UAA sequences (64) and appear to represent allelic pocket variation (Supplemental 2D). Available information suggests that at position 70 the MHC-I alleles in the cartilaginous nurse shark, banded houndshark, and clearnose skate tend to possess either a large tryptophan or a small alanine or serine (Supplemental 2Ba, 2D). This is different from the polymorphism typically found at position 70 in tetrapod species (16, 57) and probably causes distinct allelic differences in C pocket sizes, the reason for which is unclear.

High allelic polymorphism previously reported for shark MHC-I (15, 64) largely maps, as predicted (15), to the peptide binding groove as determined in the current study (Supplemental 2D).

Conserved hydrogen bond networks for binding peptide ligand termini

A set of MHC-I residues typically participating in hydrogen bonding networks with the peptide ligand main chain termini (65) are well conserved throughout classical MHC-I sequences, including those of sharks (15, 16, 64, 66). The best conserved of these residues are Y7, Y59, (R/Y)84, T143, K146, W147, Y159, and Y171 (Supplemental 2Ba),

but the relatively well conserved (E/N/Q)63 and (D/N/S)77 also tend to participate in such hydrogen bonding (65, 67). Among these residues, especially the orientations of Y7, Y59, T143, Y159, and Y171 are very well conserved (Fig. 4A) (41, 65), and four of these five residues are tyrosines that form part of the A pocket (Fig. 4Ab) where the P1 side chain experiences relatively few restrictions because it points out of the groove. The Y7 side chain can reach from α1 domain β-strand S1 to the A pocket because there is no interference by a side chain from the conserved MHC-I–specific residue G26 in β-strand S2 (Fig. 4Aa). The A pocket is also characterized by the rather well-conserved MHC-I–specific residue W167 that blocks the groove (Fig. 4Aa). In contrast to the A pockets, the F pockets show more plasticity in agreement with their engulfing of several possible amino acid side chains, and the plasticity of the F pocket can involve considerable variations in the orientations of the above-listed conserved peptide-binding residues (e.g., K146 in Fig. 4Aa) (62, 68, 69).

The conserved hydrogen bond networks for binding the peptide ligand N and C termini are shown individually for shark pUAA and other representative pMHC-I structures in Fig. 4B, exemplifying some variation in the binding of the peptide ligand C terminus (note that the resolution of the elucidated frog pUAA structure is not high enough for identifying water molecules in the A pocket hydrogen bond network) (57). Unlike the situation in most pMHC-Is, in shark pUAA the N77 side chain does not form a hydrogen bond with the peptide main chain (Fig. 4B), seemingly because the respective part of the peptide is elevated by the W73 residue (Fig. 3B). Whether the differences for binding the peptide ligand C terminus shown in Fig. 4B represent different tendencies per species, or mostly reflect HC-allelic and peptide ligand differences, can only be answered after more pMHC-I structures per species have been studied.

Impressively conserved interactions between β_2-m and the $\alpha 1\alpha 2$ domain

The contact area between β_2-m and the $\alpha 1\alpha 2$ domain in shark pUAA shows many features that are found throughout pMHC-Is but have received little attention. The most impressively conserved feature is the insertion of a β_2-m FB56+WB60 (the "B" represents β_2-m) large hydrophobic knob into a pleat of the $\alpha 1\alpha 2$ domain β-sheet floor, a binding structure involving many residues and several hydrogen bonds. Another rather well-conserved interface feature, although not well conserved in precise orientation, concerns hydrogen bond contacts between the side chains of β_2-m DB53 and $\alpha 1$ domain (K/R)48.

Supplemental 3A and 3B list all residues that according to PDBePISA software analysis are part of the $\alpha 1\alpha 2$-to-β_2-m interfaces of shark pUAA and representative pMHC-Is of carp, frogs, chickens, and humans, whereas Fig. 5A–C depicts the interactions between these domains in the shark pUAA structure. The dominant contact of β_2-m to HC concerns the binding of the β_2-m stretch comprising positions 53–60, which includes β-strand S4b and most of the S4S5-loop, to a pleat in the $\alpha 1\alpha 2$ β-sheet with which the position 53–58 stretch of β_2-m stretch runs parallel; for convenience, in the current study, this $\alpha 1\alpha 2$ pleat with HC residue 9 as a top ridge residue is named the "pa9 pleat" (pa for peptide binding domain $\alpha 1$),

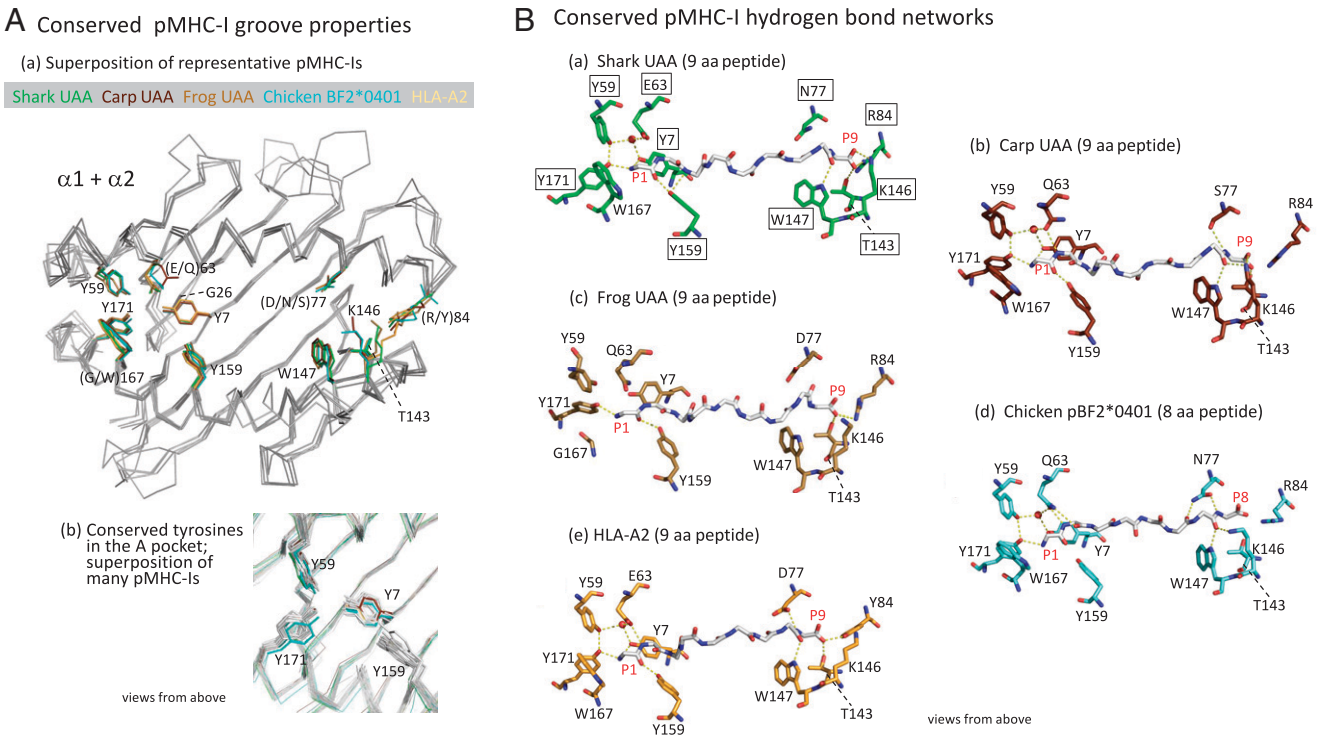

FIGURE 4. Evolutionary conservation of groove properties and peptide ligand binding modes. (**A**) Conserved groove properties. (A**a**) Superposition of representative pMHC-I $\alpha 1\alpha 2$ domain structures (peptide ligands not shown) with the side chains of (relatively) well-conserved A and F pocket residues or of the residues at their corresponding positions highlighted in a sticks format; only these side chains are given molecule-specific colors. (A**b**) The A pocket region of the figure as in (A**a**) but with superposition of many additional pMHC-Is (gray only; for PDB accessions numbers, see *Materials and Methods*) and only highlighting the well-conserved residues Y7, Y59, Y159, and Y171. (**B**) Conserved pMHC-I hydrogen bond networks. For the individual pMHC-I molecules (B**a**–B**e**) superimposed in (A**a**), the peptide ligand main chains and the HC residues Y7, Y59, (E/Q)63, (D/N/S)77, (R/Y)84, T143, K146, W147, Y159, (G/W)167, and Y171 are shown in a sticks format, together with an important water molecule (red sphere) in the A pocket and polar contacts. Boxed in (B**a**) are those residue positions that, although not necessarily in all pMHC-Is, are common in pMHC-Is for forming a hydrogen bond network with the peptide ligand.

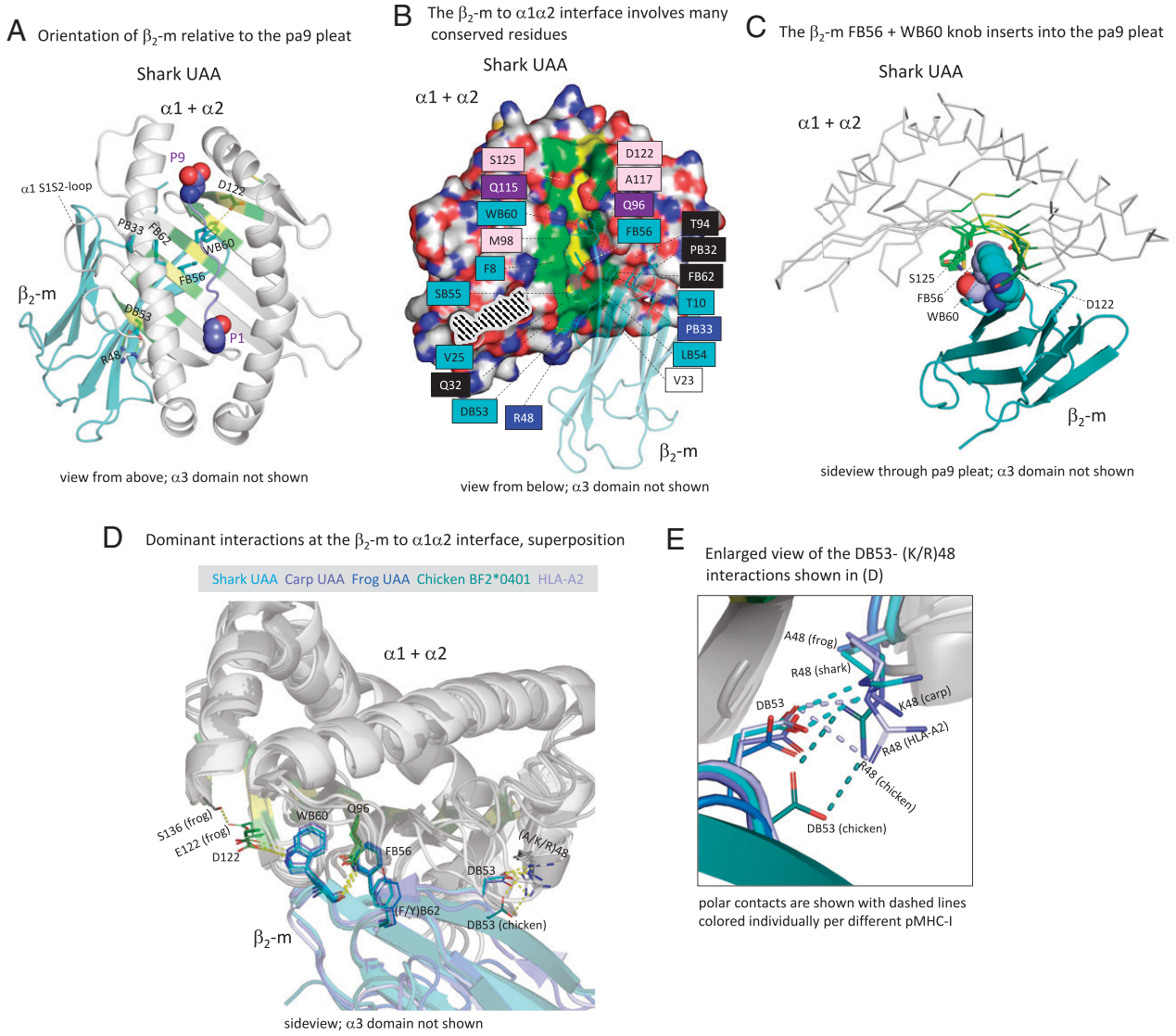

FIGURE 5. Evolutionary conservation of features at the interface between β_2-m and $\alpha1\alpha2$ domains. (**A**) Orientation of β_2-m relative to the pa9 pleat. The shark pUAA β_2-m and $\alpha1\alpha2$ domains are shown in a transparent cartoon format with some of the interacting residue side chains highlighted in a sticks format and the main chain atoms of peptide ligand residues P1 and P9 highlighted in a spheres format. The major contact site involves the β_2-m stretch DB53-to-WB60 and the $\alpha1\alpha2$ domain pa9 pleat (yellow for the top ridge residues, green for the lower ridge residues) with polar contacts at the DB53 and WB60 ends. (**B**) The shark pUAA $\alpha1\alpha2$-to-β_2-m interface involves many residues with conserved identities or characteristics, especially at the pa9 pleat contact region and a therewith continuous contact region that includes $\alpha2$ domain T94 and β_2-m PB32, PB33, and (F/Y)B62. Many of the indicated residue names are shaded with non-white colors, which are based on estimated conservation patterns as explained in Supplemental 2B: black, inherited from a presumed MHC homodimer ancestor; dark blue, ancestral to the I-$\alpha1+\beta_2$-m/IIα lineage; purple, ancestral to the I-$\alpha2$+I-$\alpha3$/IIβ lineage; light blue, characteristic for the I-$\alpha1+\beta_2$-m lineage; and pink, characteristic for the I-$\alpha2$+I-$\alpha3$ lineage. The $\alpha1\alpha2$ domain is indicated in a surface format with only yellow for pa9 pleat top ridge residues (the ability to see yellow in this figure is evidence of the pleat being open) and element coloring for the other $\alpha1\alpha2$ domain residues with red, blue, and gold for O, N, and S atoms, respectively; dark and light green for the C atoms of the residues of the pa9 pleat "pa8" and "pa10" lower ridges, respectively; and white for the other C atoms. The β_2-m domain is shown in a cyan transparent cartoon format with side chains of highlighted residues in an element color sticks format. The black and white striped area depicts the contact region between the $\alpha1\alpha2$ and $\alpha3$ domains. Residue S125 does not directly contact β_2-m but represents a conserved property of the pa9 pleat (Supplemental 2Ba). (**C**) The β_2-m FB56+WB60 residues (shown in an individual, element color spheres format) insert into the pa9 pleat, which can easily be seen from this angle with the $\alpha1\alpha2$ domain shown in a ribbon format [side view from the $\alpha2$-helix side; coloring as in (B)] and the side chains of the pa9 pleat pa8 and pa10 lower ridges in a sticks format. For the yellow-colored residues at the top ridge of the pa9 pleat, the side chains are not shown, as they all point upward and do not form part of the contact site. (**D**) Superposition, based on superimposing of $\alpha1\alpha2$ domains, of shark pUAA and representative other pMHC-I structures. Coloring similar to (C), except for using different colors for the individual β_2-m domains. There is a high level of positional conservation of Q96, D122, FB56, WB60, and (F/Y)B62, including polar contacts of WB60 with Q96 and D122 (see also Supplemental 4A); that is, except in frogs, in which E122 bends away and makes a polar contact with S136. In comparison, at the (A/K/R)48 and DB53 side of the β_2-m-to-$\alpha1\alpha2$ interface more variation is observed. (**E**) Enlarged view, compared with (D), of the region with DB53 and (A/K/R)48, with dashed lines colored per individual structure indicating polar contacts between DB53 and (K/R)48 residues.

and in Fig. 5 its top ridge and lower ridge residues are highlighted with yellow and green, respectively. Along this contact region many β_2-m and $\alpha1\alpha2$ residues with conserved identities or features are found, most of them specific for MHC-I as highlighted in Fig. 5B where text-box colors relate to patterns of conservation (compare with Supplemental 2B). At one end of the β_2-m B53–B60 stretch, DB53 forms a salt bridge with $\alpha1$ domain R48, and at the other end of the stretch WB60 forms hydrogen bonds with $\alpha2$ domain Q96

and D122 [already reported for pHLA-A2 by Saper et al. (31)]. The β_2-m molecule sweeps to under the "α1 helix half" of the α1α2 domain and the β_2-m to α1α2 interface additionally involves binding of β_2-m FB62 and S2S3-loop (including PB32 and PB33) to the α1 domain β-strand S1 C-terminal end plus S1S2-loop, and a direct contact between FB62 and the pa9 pleat (Fig. 5A, 5B, 5D; Supplemental 4A). The most pronounced β_2-m to α1α2 interaction is the insertion of the large hydrophobic knob consisting of β_2-m FB56 and WB60 into the pa9 pleat (Fig. 5C) [already noted in pHLA-A2 by Saper et al. (31)]. Fig. 5D shows that this dominant interaction, including the Q96-WB60 and D122-WB60 hydrogen bonds, is conserved in large detail between shark pUAA and other representative pMHC-Is, although in frog pUAA the D122-WB60 hydrogen bond is absent and an S136-E122 polar contact is found instead. Among pMHC-Is, also the (F/Y)B62 orientation is well conserved (Fig. 5D). Furthermore, besides the residues highlighted in Fig. 5D, a relatively large set of additional β_2-m and α1α2 residues near the FB56+WB60 and (F/Y)B62 contact sites show conserved identities or characteristics, although displaying more variation regarding the precise orientation of residues (compare Fig. 5B with Supplemental 2B, 4A).

Regarding orientation, the salt bridge between β_2-m DB53 and α1 domain R48 reported for pHLA-A2 by Saper et al. (31) is relatively poorly conserved (Fig. 5E) (70), and frog pUAA does not even possess a basic residue at that α1 position; however, the side chain of the highly conserved DB53 probably can form a hydrogen bond contact with an α1 domain (K/R)48 residue side chain in most pMHC-Is (Fig. 5E; Supplemental 2B).

A highly conserved contact between β_2-m and the α3 domain

Supplemental 3C and 3D list all residues that according to PDBePISA software analysis are part of the α3-to-β_2-m interfaces of shark pUAA and are representative pMHC-Is of carp, frogs, chickens, and humans. Among these interactions, only the hydrogen bond between β_2-m YB10 and α3 P235 and a stacked ring contact of P235 with β_2-m (F/H/Y)B26 are well conserved (Fig. 6) (31, 70).

Among pMHC-Is, there are differences in the number of polar α3-to-β_2-m interactions (Supplemental 3D) and variation in the relative positions of the α3 domain β-strands S4 and S5 (Supplemental 4Ba). Other than β_2-m YB10 and (F/H/Y)B26, and α3 residue P235, there are additional interface residues with interesting conservation patterns (Supplemental 3Bb), although none of them is perfectly conserved, and their structural orientations are compared in Supplemental 4Bb.

Evolutionary developments from pMHC-I in primitive jawed vertebrates toward mammalian pMHC-I

Some shark pUAA structural motifs that are different from mammalian pMHC-Is probably represent a more primitive state, as can be assessed by comparison of MHC sequences (Supplemental 2B) and pMHC-I and pMHC-II structures. We dedicated a separate paper to a detailed pMHC-I with pMHC-II comparison (71) and will only summarize a few findings of I–II comparisons here. None of the changes within pMHC-I evolution from shark to human appears to be very dramatic, but they are nevertheless interesting. 1) The α3 domain orientation in primitive pMHC-Is is more similar to that of the corresponding II-β2 domains in pMHC-IIs (Supplemental 4C). 2) The peptide-binding residue R84 in primitive MHC-I was replaced by Y84 in higher vertebrates (Fig. 4B), as already observed by others (66, 72). 3) In the α1 domain H1 helix region of MHC-I in placental mammals a single residue was deleted, probably at position 54a (Supplemental 2Ba), which appears to have resulted in the H1 α-helix as found in, for example, shark pUAA being replaced by a more tightly wound 3_{10}-helix structure (73) to compensate for the loss of chain length (Fig. 7A; Supplemental 2Aa, 2Ba). 4) Q49 found in the MHC-I α1 domain of primitive animals was lost in Rhipidistia (lungfishes plus tetrapods) (Supplemental 2Ba) and in shark pUAA appears to stabilize the A pocket side of the groove by making polar contacts with Q32 and R48 main chains (Fig. 7A). 5) The S1S2-loop bends downward in the MHC-I α1 domain of primitive animals, whereas in mammals the loop bends upward, leading to a decreased interaction between HC and β_2-m at this position (41, 54) while forming an R14-D39 interloop salt bridge within the α1 domain (Fig. 7B) (31). 6) In pMHC-I of placental mammals the S2-continuous part of the α2 domain S1S2-loop was repositioned to above the S1-continuous part, and the S4-continuous part of the α2 domain S3S4-loop was repositioned to above the S3-continuous part, while residues

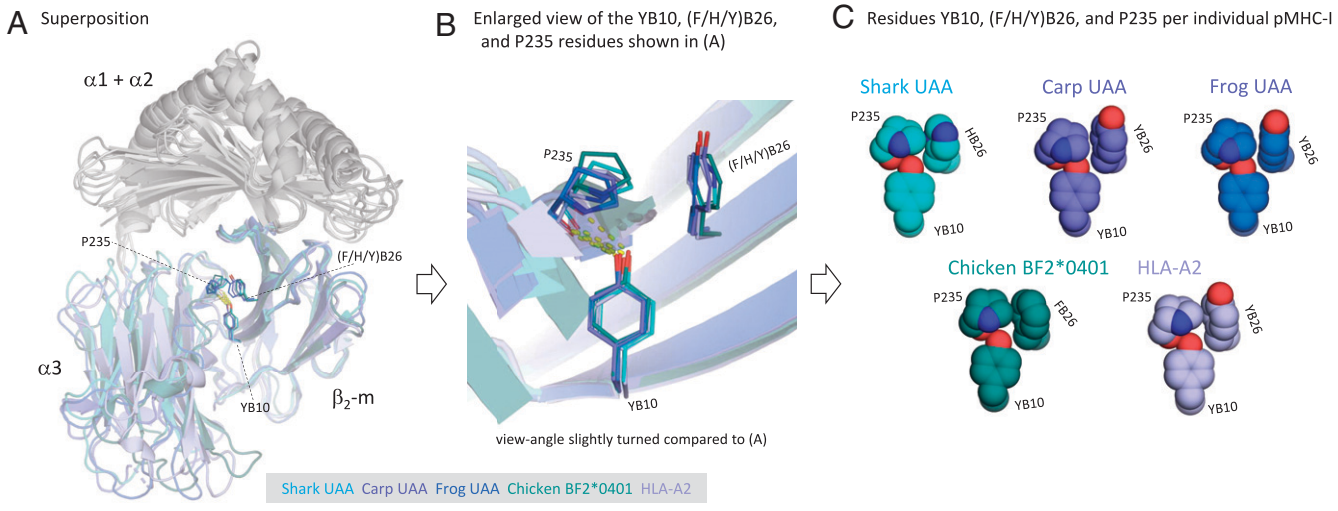

FIGURE 6. Evolutionary conservation of features at the interface between β_2-m and α3 domains. (**A**) Conserved β_2-m-to-α3 interactions between YB10, (F/H/Y)B26, and P235, with polar contact between YB10 side chain and P235 main chain and a ring-ring contact between P235 and (F/H/Y)B26, as shown by superposition (based on superimposing of β_2-m) of shark pUAA and representative pMHC-Is (A and **B**) and by individual presentation of the residue sets in a spheres format (**C**). For YB10 and (F/H/Y)B26 only the side chains plus Cα are shown, whereas for P235 all atoms are shown. (B) is an enlarged view of a part of the superposed structures shown in (A).

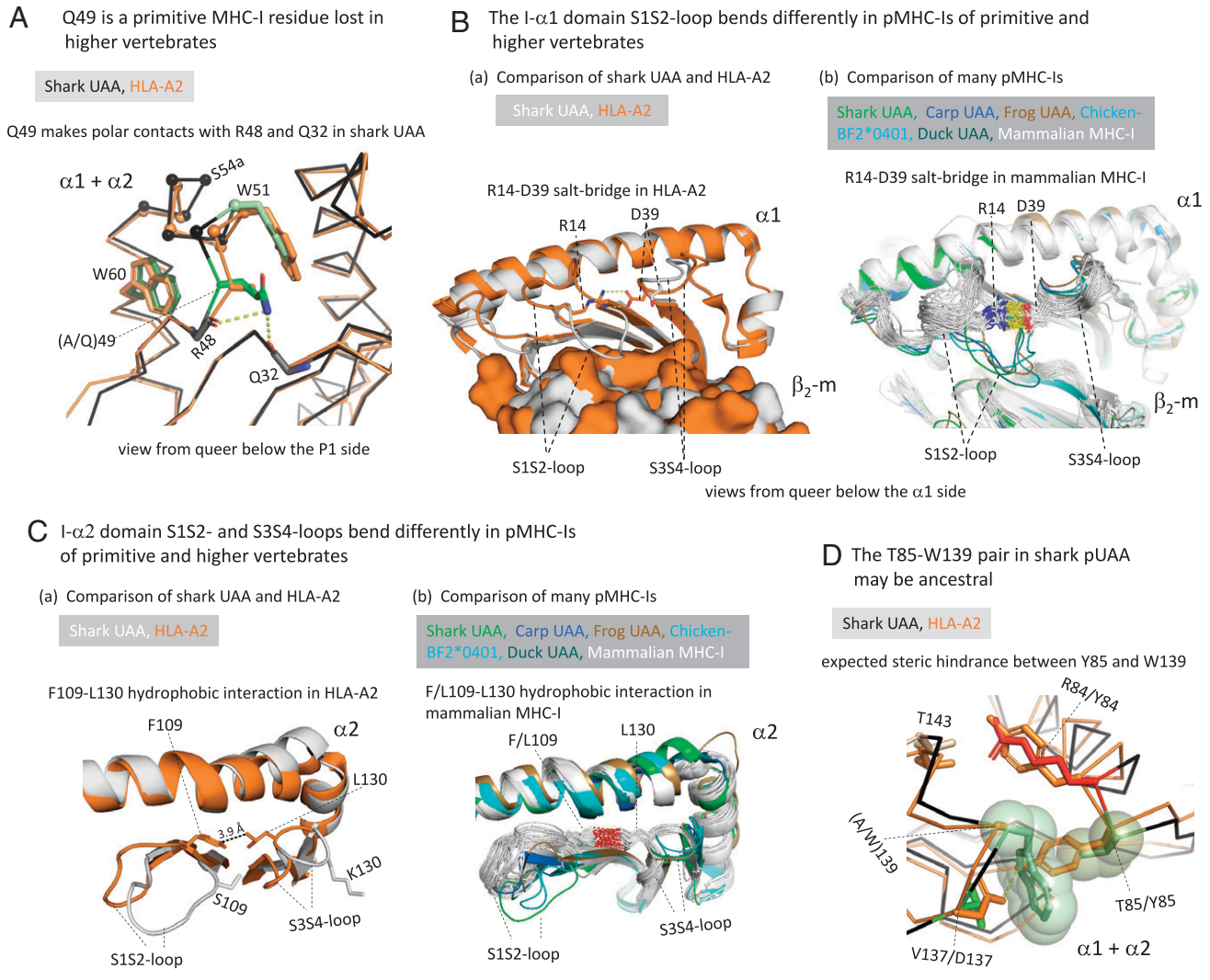

FIGURE 7. Shark pUAA features that may be primitive in comparison with mammalian pMHC-I. (**A**) In comparison with mammalian pMHC-I such as pHLA-A2, shark pUAA possesses an extra residue at position 54a, allowing a more loosely wound α1 domain H1 helix. The shark pUAA Q49 residue (side chain shown in a sticks format) makes polar contacts with the main chains of the positions 32 and 48 residues (only their main chains are shown in a sticks format). The W51 and W60 side chains are shown for orientation. (**B**) The α1 domain S1S2-loop bends differently in pMHC-Is of primitive and higher vertebrates, as shown by comparison between shark pUAA and pHLA-A2 (B**a**), and between multiple pMHC-Is (B**b**). The highly conserved R14 and D35 in mammalian MHC-I form a stable salt bridge (dashed yellow lines), which locks the α1 domain S1S2-loop and S3S4-loop together; this *(Figure legend continues)*

(L/F)109 and L130 were acquired forming a hydrophobic couple in contact range of each other (their distance in the depicted pHLA-A2 structure is <4 Å) (Fig. 7C) and of other hydrophobic residues (Supplemental 4D). 7) An interacting T85 and W139 pair of residues is found in shark pUAA (Fig. 7D), which may or may not be ancestral given their distribution among MHC-I and MHC-II peptide binding domain sequences (Supplemental 2Ba). Steric hindrance is expected to prohibit compatibility of shark W139 with the (F/Y)85 residue found in more evolved species (Fig. 7D), but whether the evolutionary changes at positions 85 + 139 had a functional effect can only be speculated. In pHLA-A2, Y85 makes a polar contact with D137, which is common among mammalian pMHC-Is (for sequence conservation patterns, see Supplemental 2Ba). 8) Ancient β_2-m may have possessed TB65 and (K/R)B66 (Supplemental 2Bb), as found in shark pUAA where the side chains of these residues make interstrand connections through polar contacts with the β_2-m HB26 side chain and residue B37 main chain, respectively (Fig. 7E). The shark β_2-m RB66-to-residue B37 interaction connects the two β_2-m β-sheets, as do the corresponding KB66-to-residue B37 interactions in carp and frogs β_2-m (Fig. 7E). However, in carp and frog β_2-m, different from shark β_2-m, the TB65 residues do not form polar contacts with the B26 residue side chain (Fig. 7E). 9) Ancient I-α3 may have possessed (K/R)245 (Supplemental 2Bb) as found in shark pUAA where the R245 side chain makes a polar contact with α3 V215 main chain connecting the two β-sheets (Fig. 7F). HC residue 245 corresponds with β_2-m residue B66 (compare Fig. 7E and 7F; Supplemental 2Bb), and, since at the corresponding position in MHC-II IgSF domains (K/R) residues are rare (Supplemental 2Bb), they may have been acquired independently in primitive β_2-m and I-α3. 10) Ancient pMHC-I presumably possessed I-α3 domain T206, as the residue is common in MHC-I of cartilaginous fish, ray-finned fish, and coelacanth (Supplemental 2Bb). In shark pUAA and carp pUAA, this threonine seems to help to attach the I-α3 domain S4S5 loop by an intradomain polar contact with the N236 side chain (Fig. 7G). Additionally, T206 makes an interdomain polar contact with the β_2-m residue B12 main chain (Fig. 7G), and so contributes to HC-to- β_2-m binding.

There are also MHC-I motifs that are specifically shared among Elasmobranchii and Holocephali, or only among Elasmobranchii, which may have been established in a cartilaginous fish species after cartilaginous fish separated from bony animals (Supplemental 2B).

Mutation of shark β_2-m YB10, DB53, FB56, or WB60 inhibits stable pMHC-I complex formation

The four residues YB10, DB53, FB56, and WB60 are highly conserved among β_2-m sequences and participate in conserved interactions with HC (Figs. 5, 6). To investigate the importance of these four residues for pMHC-I complex formation, in shark β_2-m each of them was substituted individually for an alanine. Complex formation using wild-type or mutant β_2-m together with HC (Gici-UAA*0101) and peptide pep56 was analyzed using gel filtration for the renaturing protocol product (Fig. 8A), followed by anion-exchange chromatography for the isolated pMHC-I complexes (Fig. 8B). Fig. 8A suggests that all four β_2-m mutants had some ability to participate in pMHC-I complex formation, although at a much lower level than wild-type β_2-m, whereas Fig. 8B shows that none of these complexes was stable.

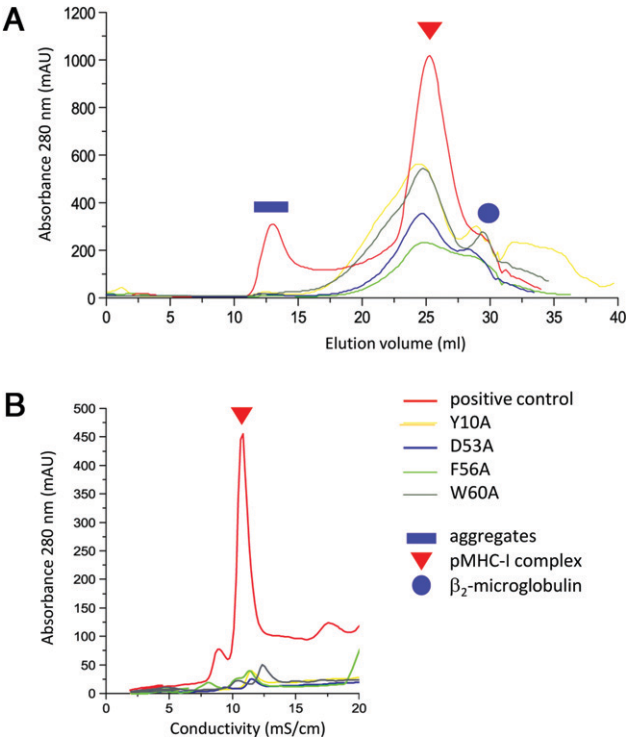

FIGURE 8. Assembly and stabilization assay of shark pMHC-I complexes consisting of Gici-UAA*0101, pep56 peptide, and wild-type or mutant β_2-m, after in vitro refolding. Curves for the wild-type (positive control) and four mutant β_2-ms (YB10, DB53, FB56, and WB60 mutated to alanine) are shown with individual colors. (**A**) Gel filtration chromatograms of the refolded products obtained using a Superdex 200 10/300 GL column. Aggregates, correctly refolded pMHC-I complex, and excess β_2-m are indicated using a blue solid box, red solid triangle, and blue solid circle, respectively. The heights of the pMHC-I complex peaks are indicative for the efficiencies of the respective β_2-m mutants to support pMHC-I complex formation. (**B**) Anion-exchange chromatography results for the isolated pMHC-I complexes. A higher peak indicates better stability. The results reveal that the four residues YB10, DB53, FB56, and WB60 of shark β_2-m are critical for stable pMHC-I complex formation.

Discussion

The present study closes an important gap in knowledge of the evolution of pMHC-I structures by elucidating a pMHC-I structure in cartilaginous fish. Arguably, it is also the first study to extensively compare the overall structures of divergent pMHC-Is. Previously,

salt bridge does not exist in non-mammalian vertebrates, and their α1 S1S2-loops bend toward β_2-m. (**C**) The α2 domain S1S2- and S3S4-loops bend differently in pMHC-Is of primitive and higher vertebrates, as shown by comparison between shark pUAA and pHLA-A2 (**Ca**), and between multiple pMHC-Is (**Cb**). The conformation of the S1S2- and S3S4-loops in eutherian mammal pMHC-I α2 domains involves a hydrophobic interaction (dashed red lines) between the MHC-I–specific residues (F/L)109 and L130. (**D**) The T85-W139 pair in shark UAA may be ancestral. Transparent spheres presentation of the shark pUAA W139 and pHLA-A2 Y85 residues reveals that steric hindrance would probably prohibit coexistence of these two residues. In pHLA-A2, Y85 makes a polar contact with D137. Residues (R/Y)84 and T143 are highlighted for orientation. (**E**) Polar contact between (K/R)B66 side chain and position 37 main chain in β_2-m of primitive vertebrates, and polar contact between shark TB65 and HB26 side chains. The sticks format highlights residue side chains for positions B26, B65, and B66, and the residue main chain for position B37. (**F**) The polar contact between (K/R)245 side chain and position 215 main chain as seen in the shark pUAA α3 domain probably is a primitive pMHC-I feature. The sticks format highlights the residue side chain for position 245, and the residue main chain for position 215. (**G**) Polar contacts of T206 side chain with N236 side chain and β_2-m position 12 main chain as found in shark pUAA and carp pUAA probably are primitive pMHC-I features. The sticks format highlights residue side chains for positions 206 and 236, and the residue main chain for position B12.

the most comprehensive analysis of pMHC-I structural organization had been the study by Saper et al. (31), whereas later structural studies mostly concentrated on the peptide binding domains. The most important contribution of the current study to the general understanding of pMHC-I structures probably is our analysis of the H chain with β_2-m interactions. At the HC-to-β_2-m interface three major binding patches can be distinguished, represented by the conserved β_2-m residues YB10 (Fig. 6), DB53 (Fig. 5E), and FB56+WB60 (Fig. 5C). The combination of β_2-m residues PB32, PB33, and (F/Y)B62 could be considered as part of an additional, evolutionary older, binding patch with less pronounced binding features, or as part of the "FB56+WB60" patch with which it is continuous (Fig. 5A–D; Supplemental 3A, 3B, 4A, 4E). All three major binding patches, each including intermolecular hydrogen bonds (Figs. 5, 6; Supplemental 3B, 3D), were already analyzed in detail for pHLA-A2 by Saper et al. (31) and, although in lesser detail, described for mouse pH2-Kb by Fremont et al. (61) in 1992. In 2013, Hee et al. (70) compared chicken and mammalian pMHC-I structures and noted the conservation of the three patches but did not show the structures of the YB10 or FB56+WB60 patches. Nonetheless, Hee et al. (70) did present a detailed analysis of the DB53 patch, showing that β_2-m DB53 and α1 R48 residues form salt bridges in the investigated chicken and mammalian pMHC-I structures, although in various orientations (as we confirmed; Fig. 5E). However, to our knowledge, since the analysis of pHLA-A2 by Saper et al. (31), there have been no reports describing that the β_2-m FB56+WB60 hydrophobic knob penetrates a pleat of the $\alpha1\alpha2$ floor (Fig. 5C). This pleat penetration, whereby both FB56 and WB60 make direct contact with the main chains of the residues at the pleat top ridge, appears to be perfectly conserved among pMHC-Is (Fig. 5D; Supplemental 4A) and was not found in pMHC-IIs (74). Essentially, in general, previous studies have not been fully aware that many of the interactions originally observed for binding of β_2-m to $\alpha1\alpha2$ in pHLA-A2 by Saper et al. (31) are (rather) well conserved throughout pMHC-Is. Those conserved interactions at the β_2-m-to-$\alpha1\alpha2$ interface involve the (rather well) conserved residues α1 F8, T10, V25, Q32, and (K/R)48; α2 T94, Q96, M98, Q115, (A/G)117, D122, and (A/S/T)125; and β_2-m PB32, PB33, DB53, (M/L)B54, (A/G/S)B55, FB56, WB60, and (F/Y)B62 (Fig. 5; Supplemental 2, 3A, 3B, 4A).

In stark contrast to the $\alpha1\alpha2$-to-β_2-m interfaces, the $\alpha3$-to-β_2-m interfaces of shark pUAA and other pMHC-Is are not characterized by a multitude of conserved interactions. However, an interaction involving β_2-m residues YB10 and (F/H/Y)B26, and α3 residue P235, is well conserved (Fig. 6; Supplemental 4B). The conservation of the hydrogen bond between the YB10 side chain and P235 main chain (Fig. 6B) was noted previously upon analysis of chicken and mammalian pMHC-Is (70).

By alanine substitution analysis, we determined that the four conserved residues of shark β_2-m that make the most pronounced interactions with the H chain, that is, YB10, DB53, FB56, and WB60, are critical for stable pMHC-I complex formation (Fig. 8). The importance of WB60 for pMHC-I complex formation had previously been reported for human β_2-m (33), and the importance of DB53 had been suggested by a reduction in the stabilizing ability of human β_2-m on murine pMHC-I after this residue was mutated (32). However, to our knowledge, we are the first to analyze the importance of the YB10 and FB56 residues for pMHC-I complex formation, which illustrates how relatively little attention has been given in previous studies to the interactions between β_2-m and H chain. The observed importance of YB10 is especially interesting because it suggests that (the mode of) binding of β_2-m to not only $\alpha1\alpha2$ (32, 33) but also to the α3 domain is important for stable pMHC-I complex formation. To our knowledge, the latter has not been shown in such a direct manner before, although it was established that the presence of the α3 domain is necessary for β_2-m to support peptide binding by the $\alpha1\alpha2$ domain (75) and that a change in the α3 domain could affect both binding of β_2-m and the presentation of pMHC-I at the cell surface (76).

The pMHC-I refolding experiments with nurse shark Gici-UAA*0101 showed that 9-aa peptide ligands could be bound depending on their P2 and P9 (P_Ω) residues, and possibly their intrapeptide folding properties (Figs. 1, 3; Supplemental 1A), which is reminiscent of findings for other species and can be HC-allele–dependent (77, 78). Preference for a hydrophobic anchor residue at the peptide C-terminal position (P_ω), as found with leucine or valine in the case of Gici-UAA*01 (Fig. 1), is common among pMHC-I complexes in mammals and other jawed vertebrates (e.g., 36, 55, 57, 77, 79, 80), although for some MHC-I alleles other P_ω preferences have been observed (77, 79). Selection for peptide P2 and P9 residues is consistent with the shark pUAA binding groove having B and F pockets for binding the P2 and P9 side chains (Fig. 3C), and the overall orientation of the pep56 peptide ligand and the organization of the groove pockets in shark pUAA are reminiscent of pMHC-I structures known for other species (Figs. 3, 4). Sets of residues for binding the peptide ligand termini, especially for binding the N terminus in the A pocket, are impressively conserved between shark pUAA and other pMHC-Is (Fig. 4). Conservation of A and F pocket organization throughout pMHC-Is of widely diverged jawed vertebrates has been noted before (41, 54). Some unique features were also observed (e.g., Fig. 3B, 3F), but at least some of those appear to be HC-allele-specific or peptide-specific rather than general characteristics of pMHC-I in sharks.

Several evolutionary changes from shark to human pMHC-I could be distinguished, such as the replacement of the R84 residue involved in peptide ligand main chain binding for Y84 (Fig. 4B) (66), a change in α3 domain orientation (Supplemental 4C) (41, 54), and a few other structural changes (Fig. 7). Additionally, some sequence features could be distinguished that were specifically established in cartilaginous fish (Supplemental 2B). These animal-clade–specific pMHC-I differences, all of which seem relatively minor, can probably not be explained at the functional level yet because the precise mechanisms of pMHC-I complex formation and peptide editing are still unknown. Notably, with regard to the R84 residue in primitive vertebrates (66), Xiao et al. (56) found for a chicken pBF2*1201 structure that the R84 side chain was rotated outward and so allowed the peptide ligand to extend one residue beyond the F pocket, whereas the structure appeared to be stabilized by a hydrogen bond between the R84 side chain and the P_Ω carboxyl group. The authors speculated that this organization may be common in pMHC-Is of primitive vertebrates (56). However, even among chicken pMHC-Is such extensions beyond the F pocket are not very common (79), whereas in mammalian pMHC-I extensions are more common than originally thought (81). Furthermore, in mammalian pMHC-Is the Y84 residue side chain can also rotate away from the F pocket and then allow peptide extensions, although unlike in chicken pBF2*1201 this was found to be accompanied by a shift in the α1 domain helix orientation [summarized in Xiao et al. (56)]. In summary, there is probably not enough evidence yet to conclude that the evolutionary exchange of R84 for Y84 had an important impact on the modes of peptide binding. In the current study we only investigated nonamer peptides, but in the future we hope to also analyze the binding of longer peptides to shark MHC-I.

A big question in pMHC-I science is how the synergistic binding of β_2-m, HC, and peptide (82, 83) can be explained mechanically. Whereas β_2-m is stable when alone, HC on its own is unstable (e.g., Fig. 1) and only structures of HC together with β_2-m and peptide ligand, or HC together with β_2-m and tapasin (aka TAP binding protein [TAPBP]) or TAPBPR (TAPBP-related, aka tapasin-like), are

known (84–87); hence, it is not understood how β_2-m affects HC at the structural level. The precise conservation of several of the major interactions at the HC-to-β_2-m interfaces (Figs. 5, 6) strongly suggests that β_2-m binding is about a mechanism and not just about binding. This is further supported by mouse HC having a higher affinity for human β_2-m than for mouse β_2-m (88), as it reveals that nature has not opted for β_2-m with the highest possible HC affinity. We speculate that in β_2-m–free HC the pa9 pleat may be closed by coverage of side chains of residues at the pleat lower ridges, as found in pMHC-II (74), and that the binding of β_2-m may open the pa9 pleat and promote peptide ligand binding through a cascade of unknown interactions. In this regard, it is interesting that tapasin and TAPBPR, the genes of which are found throughout jawed vertebrates (Ref. 3 and GenBank accession numbers XP_007910636 and XP_020375342), may keep the HC binding groove open not only by providing a "scoop loop" (a kind of peptide dummy) for binding the F pocket region but also by direct interactions with the conserved residues Q115, D122, and WB60, which reside at the HC-to-β_2-m interface, at least in the case of TAPBPR (84–86, 89, 90). Although the β hairpin in TAPBPR that mediates the latter set of interactions has been portrayed as "jack hairpin," as if it helps with conformational changes observed in the $\alpha1\alpha2$ domain (86), we speculate that its primary function may be the stabilization of the HC-to-β_2-m binding while maintaining the insertion of the FB56+WB60 knob into the pa9 pleat.

Besides shark pUAA, we also determined the structure of free shark β_2-m and compared it with free β_2-m structures elucidated for other species (Supplemental 4E). Whereas the orientations of β_2-m FB56 and WB60 residues are remarkably conserved within pMHC-I structures (Fig. 5D), they show considerable variation between the free β_2-m structures. This makes discussion of a possible "induced fit" mechanism, which might trigger structural changes in the HC, complicated. Nevertheless, there are indications for the involvement of β_2-m in "tuning" the peptide binding groove—rather than being a simple "lock" for the pMHC-I complex—as, for example, shown by a recent study of our group in carp. Namely, in two carp pMHC-I structures with identical HC and peptide, but with different, naturally occurring, paralogous β_2-m variants, the peptide was bound in a different conformation (58). This finding in carp was not unexpected, since earlier reports had found that naturally occurring allelic variation in mouse β_2-m is associated with differences in peptides presented by MHC-I (91) and T cell stimulation (91, 92).

In summary, our study shows that pMHC-I complexes of highly divergent jawed vertebrate species share a near-perfect conservation of relatively large parts of the peptide binding groove and the $\alpha1\alpha2$-to-β_2-m interface, and a small patch at the $\alpha3$-to-β_2-m interface. This suggests that not much changed in pMHC-I mechanisms and functions after the evolutionary separation of cartilaginous fish and bony animals. Future studies should unravel how the conserved structures interact mechanically to support peptide binding and editing.

Acknowledgments

We acknowledge the assistance provided by the staff at the Shanghai Synchrotron Radiation Facility of China (SSRF) for technical assistance during data collection.

Disclosures

The authors have no financial conflicts of interest.

References

1. Renz, A. J., A. Meyer, and S. Kuraku. 2013. Revealing less derived nature of cartilaginous fish genomes with their evolutionary time scale inferred with nuclear genes. *PLoS One* 8: e66400.
2. Flajnik, M. F., and L. Du Pasquier. 2013. Evolution of the immune system. In *Fundamental Immunology*, 7th Ed. W. E. Paul, ed. Wolters Kluwer Health/Lippincott Williams & Wilkins, Philadelphia, PA, p. 67–128.
3. Venkatesh, B., A. P. Lee, V. Ravi, A. K. Maurya, M. M. Lian, J. B. Swann, Y. Ohta, M. F. Flajnik, Y. Sutoh, M. Kasahara, et al. 2014. Elephant shark genome provides unique insights into gnathostome evolution. [Published erratum appears in 2014 *Nature* 513: 574.] *Nature* 505: 174–179.
4. Dijkstra, J. M. 2014. T_H2 and T_{reg} candidate genes in elephant shark. *Nature* 511: E7–E9.
5. Dijkstra, J. M. 2021. A method for making alignments of related protein sequences that share very little similarity; shark interleukin 2 as an example. *Immunogenetics* 73: 35–51.
6. Ott, J. A., Y. Ohta, M. F. Flajnik, and M. F. Criscitiello. 2021. Lost structural and functional inter-relationships between Ig and TCR loci in mammals revealed in sharks. *Immunogenetics* 73: 17–33.
7. Sutoh, Y., and M. Kasahara. 2021. The immune system of jawless vertebrates: insights into the prototype of the adaptive immune system. *Immunogenetics* 73: 5–16.
8. Germain, R. N. 1994. MHC-dependent antigen processing and peptide presentation: providing ligands for T lymphocyte activation. *Cell* 76: 287–299.
9. Neefjes, J., M. L. M. Jongsma, P. Paul, and O. Bakke. 2011. Towards a systems understanding of MHC class I and MHC class II antigen presentation. *Nat. Rev. Immunol.* 11: 823–836.
10. Hashimoto, K., T. Nakanishi, and Y. Kurosawa. 1990. Isolation of carp genes encoding major histocompatibility complex antigens. *Proc. Natl. Acad. Sci. USA* 87: 6863–6867.
11. Hashimoto, K., T. Nakanishi, and Y. Kurosawa. 1992. Identification of a shark sequence resembling the major histocompatibility complex class I alpha 3 domain. *Proc. Natl. Acad. Sci. USA* 89: 2209–2212.
12. Kasahara, M., M. Vazquez, K. Sato, E. C. McKinney, and M. F. Flajnik. 1992. Evolution of the major histocompatibility complex: isolation of class II A cDNA clones from the cartilaginous fish. *Proc. Natl. Acad. Sci. USA* 89: 6688–6692.
13. Kasahara, M., E. C. McKinney, M. F. Flajnik, and T. Ishibashi. 1993. The evolutionary origin of the major histocompatibility complex: polymorphism of class II alpha chain genes in the cartilaginous fish. *Eur. J. Immunol.* 23: 2160–2165.
14. Bartl, S., and I. L. Weissman. 1994. Isolation and characterization of major histocompatibility complex class IIB genes from the nurse shark. *Proc. Natl. Acad. Sci. USA* 91: 262–266.
15. Okamura, K., M. Ototake, T. Nakanishi, Y. Kurosawa, and K. Hashimoto. 1997. The most primitive vertebrates with jaws possess highly polymorphic MHC class I genes comparable to those of humans. *Immunity* 7: 777–790.
16. Hashimoto, K., K. Okamura, H. Yamaguchi, M. Ototake, T. Nakanishi, and Y. Kurosawa. 1999. Conservation and diversification of MHC class I and its related molecules in vertebrates. *Immunol. Rev.* 167: 81–100.
17. Ohta, Y., K. Okamura, E. C. McKinney, S. Bartl, K. Hashimoto, and M. F. Flajnik. 2000. Primitive synteny of vertebrate major histocompatibility complex class I and class II genes. *Proc. Natl. Acad. Sci. USA* 97: 4712–4717.
18. Ohta, Y., T. Shiina, R. L. Lohr, K. Hosomichi, T. I. Pollin, E. J. Heist, S. Suzuki, H. Inoko, and M. F. Flajnik. 2011. Primordial linkage of *β2-microglobulin* to the MHC. *J. Immunol.* 186: 3563–3571.
19. Malmstrøm, M., M. Matschiner, O. K. Tørresen, B. Star, L. G. Snipen, T. F. Hansen, H. T. Baalsrud, A. J. Nederbragt, R. Hanel, W. Salzburger, et al. 2016. Evolution of the immune system influences speciation rates in teleost fishes. *Nat. Genet.* 48: 1204–1210.
20. Wilson, A. B. 2017. MHC and adaptive immunity in teleost fishes. *Immunogenetics* 69: 521–528.
21. Dijkstra, J. M., and U. Grimholt. 2018. Major histocompatibility complex (MHC) fragment numbers alone—in Atlantic cod and in general—do not represent functional variability. *F1000 Res.* 7: 963.
22. Hughes, A. L., and M. Nei. 1989. Evolution of the major histocompatibility complex: independent origin of nonclassical class I genes in different groups of mammals. *Mol. Biol. Evol.* 6: 559–579.
23. Adams, E. J., and A. M. Luoma. 2013. The adaptable major histocompatibility complex (MHC) fold: structure and function of nonclassical and MHC class I-like molecules. *Annu. Rev. Immunol.* 31: 529–561.
24. Dijkstra, J. M., U. Grimholt, J. Leong, B. F. Koop, and K. Hashimoto. 2013. Comprehensive analysis of MHC class II genes in teleost fish genomes reveals dispensability of the peptide-loading DM system in a large part of vertebrates. *BMC Evol. Biol.* 13: 260.
25. Grimholt, U., K. Tsukamoto, T. Azuma, J. Leong, B. F. Koop, and J. M. Dijkstra. 2015. A comprehensive analysis of teleost MHC class I sequences. *BMC Evol. Biol.* 15: 32.
26. Dijkstra, J. M., T. Yamaguchi, and U. Grimholt. 2018. Conservation of sequence motifs suggests that the nonclassical MHC class I lineages CD1/PROCR and UT were established before the emergence of tetrapod species. *Immunogenetics* 70: 459–476.
27. Dijkstra, J. M., and T. Yamaguchi. 2019. Ancient features of the MHC class II presentation pathway, and a model for the possible origin of MHC molecules. *Immunogenetics* 71: 233–249.
28. Cannon, J. P., R. N. Haire, and G. W. Litman. 2002. Identification of diversified genes that contain immunoglobulin-like variable regions in a protochordate. *Nat. Immunol.* 3: 1200–1207.

29. Chen, H., S. Kshirsagar, I. Jensen, K. Lau, C. Simonson, and S. F. Schluter. 2010. Characterization of arrangement and expression of the beta-2 microglobulin locus in the sandbar and nurse shark. *Dev. Comp. Immunol.* 34: 189–195.
30. Lu, S., S. Yao, R. Chen, N. Zhang, J. Chen, F. Gao, and C. Xia. 2012. Expression, purification, crystallization and preliminary X-ray diffraction analysis of nurse shark β_2-microglobulin. *Acta Crystallogr. Sect. F Struct. Biol. Cryst. Commun.* 68: 460–463.
31. Saper, M. A., P. J. Bjorkman, and D. C. Wiley. 1991. Refined structure of the human histocompatibility antigen HLA-A2 at 2.6 Å resolution. *J. Mol. Biol.* 219: 277–319.
32. Shields, M. J., N. Assefi, W. Hodgson, E. J. Kim, and R. K. Ribaudo. 1998. Characterization of the interactions between MHC class I subunits: a systematic approach for the engineering of higher affinity variants of β_2-microglobulin. *J. Immunol.* 160: 2297–2307.
33. Esposito, G., S. Ricagno, A. Corazza, E. Rennella, D. Gümral, M. C. Mimmi, E. Betto, C. E. Pucillo, F. Fogolari, P. Viglino, et al. 2008. The controlling roles of Trp60 and Trp95 in β_2-microglobulin function, folding and amyloid aggregation properties. *J. Mol. Biol.* 378: 887–897.
34. Chen, W., Z. Jia, T. Zhang, N. Zhang, C. Lin, F. Gao, L. Wang, X. Li, Y. Jiang, X. Li, et al. 2010. MHC class I presentation and regulation by IFN in bony fish determined by molecular analysis of the class I locus in grass carp. *J. Immunol.* 185: 2209–2221.
35. Hoof, I., B. Peters, J. Sidney, L. E. Pedersen, A. Sette, O. Lund, S. Buus, and M. Nielsen. 2009. NetMHCpan, a method for MHC class I binding prediction beyond humans. *Immunogenetics* 61: 1–13.
36. Qu, Z., Z. Li, L. Ma, X. Wei, L. Zhang, R. Liang, G. Meng, N. Zhang, and C. Xia. 2019. Structure and peptidome of the bat MHC class I molecule reveal a novel mechanism leading to high-affinity peptide binding. *J. Immunol.* 202: 3493–3506.
37. Li, X., J. Liu, J. Qi, F. Gao, Q. Li, X. Li, N. Zhang, C. Xia, and G. F. Gao. 2011. Two distinct conformations of a rinderpest virus epitope presented by bovine major histocompatibility complex class I N*01801: a host strategy to present featured peptides. *J. Virol.* 85: 6038–6048.
38. Shapiro, A. L., E. Viñuela, and J. V. Maizel, Jr. 1967. Molecular weight estimation of polypeptide chains by electrophoresis in SDS-polyacrylamide gels. *Biochem. Biophys. Res. Commun.* 28: 815–820.
39. Harp, J. M., D. E. Timm, and G. J. Bunick. 1998. Macromolecular crystal annealing: overcoming increased mosaicity associated with cryocrystallography. *Acta Crystallogr. D Biol. Crystallogr.* 54: 622–628.
40. Otwinowski, Z., and W. Minor. 1997. Processing of X-ray diffraction data collected in oscillation mode. *Methods Enzymol.* 276: 307–326.
41. Chen, Z., N. Zhang, J. Qi, R. Chen, J. M. Dijkstra, X. Li, Z. Wang, J. Wang, Y. Wu, and C. Xia. 2017. The structure of the MHC class I molecule of bony fishes provides insights into the conserved nature of the antigen-presenting system. *J. Immunol.* 199: 3668–3678.
42. Collaborative Computational Project, Number 4. 1994. The CCP4 suite: programs for protein crystallography. *Acta Crystallogr. D Biol. Crystallogr.* 50: 760–763.
43. McCoy, A. J. 2007. Solving structures of protein complexes by molecular replacement with Phaser. *Acta Crystallogr. D Biol. Crystallogr.* 63: 32–41.
44. Lebedev, A. A., A. A. Vagin, and G. N. Murshudov. 2008. Model preparation in MOLREP and examples of model improvement using X-ray data. *Acta Crystallogr. D Biol. Crystallogr.* 64: 33–39.
45. Emsley, P., and K. Cowtan. 2004. Coot: model-building tools for molecular graphics. *Acta Crystallogr. D Biol. Crystallogr.* 60: 2126–2132.
46. Adams, P. D., R. W. Grosse-Kunstleve, L. W. Hung, T. R. Ioerger, A. J. McCoy, N. W. Moriarty, R. J. Read, J. C. Sacchettini, N. K. Sauter, and T. C. Terwilliger. 2002. PHENIX: building new software for automated crystallographic structure determination. *Acta Crystallogr. D Biol. Crystallogr.* 58: 1948–1954.
47. Laskowski, R. A., D. S. Moss, and J. M. Thornton. 1993. Main-chain bond lengths and bond angles in protein structures. *J. Mol. Biol.* 231: 1049–1067.
48. Kabsch, W., and C. Sander. 1983. Dictionary of protein secondary structure: pattern recognition of hydrogen-bonded and geometrical features. *Biopolymers* 22: 2577–2637.
49. Krissinel, E., and K. Henrick. 2007. Inference of macromolecular assemblies from crystalline state. *J. Mol. Biol.* 372: 774–797.
50. Becker, J. W., and G. N. Reeke, Jr. 1985. Three-dimensional structure of beta 2-microglobulin. *Proc. Natl. Acad. Sci. USA* 82: 4225–4229.
51. Bjorkman, P. J., M. A. Saper, B. Samraoui, W. S. Bennett, J. L. Strominger, and D. C. Wiley. 1987. Structure of the human class I histocompatibility antigen, HLA-A2. *Nature* 329: 506–512.
52. Halaby, D. M., A. Poupon, and J. Mornon. 1999. The immunoglobulin fold family: sequence analysis and 3D structure comparisons. *Protein Eng.* 12: 563–571.
53. Fan, S., Y. Wu, S. Wang, Z. Wang, B. Jiang, Y. Liu, R. Liang, W. Zhou, N. Zhang, and C. Xia. 2016. Structural and biochemical analyses of swine major histocompatibility complex class I complexes and prediction of the epitope map of important influenza A virus strains. *J. Virol.* 90: 6625–6641.
54. Koch, M., S. Camp, T. Collen, D. Avila, J. Salomonsen, H. J. Wallny, A. van Hateren, L. Hunt, J. P. Jacob, F. Johnston, et al. 2007. Structures of an MHC class I molecule from B21 chickens illustrate promiscuous peptide binding. *Immunity* 27: 885–899.
55. Wu, Y., J. Wang, S. Fan, R. Chen, Y. Liu, J. Zhang, H. Yuan, R. Liang, N. Zhang, and C. Xia. 2017. Structural definition of duck major histocompatibility complex class I molecules that might explain efficient cytotoxic T lymphocyte immunity to influenza A virus. *J. Virol.* 91: e02511-16.
56. Xiao, J., W. Xiang, Y. Zhang, W. Peng, M. Zhao, L. Niu, Y. Chai, J. Qi, F. Wang, P. Qi, et al. 2018. An invariant arginine in common with MHC class II allows extension at the C-terminal end of peptides bound to chicken MHC class I. *J. Immunol.* 201: 3084–3095.
57. Ma, L., N. Zhang, Z. Qu, R. Liang, L. Zhang, B. Zhang, G. Meng, J. M. Dijkstra, S. Li, and M. C. Xia. 2020. A glimpse of the peptide profile presentation by *Xenopus laevis* MHC class I: crystal structure of p*Xela*-UAA reveals a distinct peptide-binding groove. *J. Immunol.* 204: 147–158.
58. Li, Z., N. Zhang, L. Ma, L. Zhang, G. Meng, and C. Xia. 2020. The mechanism of β2m molecule-induced changes in the peptide presentation profile in a bony fish. *iScience* 23: 101119.
59. Madden, D. R. 1995. The three-dimensional structure of peptide-MHC complexes. *Annu. Rev. Immunol.* 13: 587–622.
60. Adzhubei, A. A., M. J. Sternberg, and A. A. Makarov. 2013. Polyproline-II helix in proteins: structure and function. *J. Mol. Biol.* 425: 2100–2132.
61. Fremont, D. H., M. Matsumura, E. A. Stura, P. A. Peterson, and I. A. Wilson. 1992. Crystal structures of two viral peptides in complex with murine MHC class I H-2Kb. *Science* 257: 919–927.
62. Madden, D. R., D. N. Garboczi, and D. C. Wiley. 1993. The antigenic identity of peptide-MHC complexes: a comparison of the conformations of five viral peptides presented by HLA-A2. *Cell* 75: 693–708.
63. Rognan, D., L. Scapozza, G. Folkers, and A. Daser. 1995. Rational design of non-natural peptides as high-affinity ligands for the HLA-B*2705 human leukocyte antigen. *Proc. Natl. Acad. Sci. USA* 92: 753–757.
64. Ohta, Y., E. C. McKinney, M. F. Criscitiello, and M. F. Flajnik. 2002. Proteasome, transporter associated with antigen processing, and class I genes in the nurse shark *Ginglymostoma cirratum*: evidence for a stable class I region and MHC haplotype lineages. *J. Immunol.* 168: 771–781.
65. Matsumura, M., D. H. Fremont, P. A. Peterson, and I. A. Wilson. 1992. Emerging principles for the recognition of peptide antigens by MHC class I molecules. *Science* 257: 927–934.
66. Kaufman, J., R. Andersen, D. Avila, J. Engberg, J. Lambris, J. Salomonsen, K. Welinder, and K. Skjødt. 1992. Different features of the MHC class I heterodimer have evolved at different rates. Chicken B-F and beta 2-microglobulin sequences reveal invariant surface residues. *J. Immunol.* 148: 1532–1546.
67. Bouvier, M., and D. C. Wiley. 1994. Importance of peptide amino and carboxyl termini to the stability of MHC class I molecules. *Science* 265: 398–402.
68. Chappell, P., K. Meziane, M. Harrison, Ł. Magiera, C. Hermann, L. Mears, A. G. Wrobel, C. Durant, L. L. Nielsen, S. Buus, et al. 2015. Expression levels of MHC class I molecules are inversely correlated with promiscuity of peptide binding. *eLife* 4: e05345.
69. Ayres, C. M., E. T. Abualrous, A. Bailey, C. Abraham, L. M. Hellman, S. A. Corcelli, F. Noé, T. Elliott, and B. M. Baker. 2019. Dynamically driven allostery in MHC proteins: peptide-dependent tuning of class I MHC global flexibility. *Front. Immunol.* 10: 966.
70. Hee, C. S., M. Beerbaum, B. Loll, M. Ballaschk, P. Schmieder, B. Uchanska-Ziegler, and A. Ziegler. 2013. Dynamics of free versus complexed β_2-microglobulin and the evolution of interfaces in MHC class I molecules. *Immunogenetics* 65: 157–172.
71. Wu, Y., N. Zhang, K. Hashimoto, C. Xia, and J.M. Dijkstra. 2021. Structural comparison between MHC classes I and II; in evolution, a class-II-like molecule probably came first. *Front. Immunol.* In press.
72. Kaufman, J., J. Salomonsen, and M. Flajnik. 1994. Evolutionary conservation of MHC class I and class II molecules—different yet the same. *Semin. Immunol.* 6: 411–424.
73. Mage, M. G., M. A. Dolan, R. Wang, L. F. Boyd, M. J. Revilleza, H. Robinson, K. Natarajan, N. B. Myers, T. H. Hansen, and D. H. Margulies. 2012. The peptide-receptive transition state of MHC class I molecules: insight from structure and molecular dynamics. *J. Immunol.* 189: 1391–1399.
74. Brown, J. H., T. S. Jardetzky, J. C. Gorga, L. J. Stern, R. G. Urban, J. L. Strominger, and D. C. Wiley. 1993. Three-dimensional structure of the human class II histocompatibility antigen HLA-DR1. *Nature* 364: 33–39.
75. Elliott, T., J. Elvin, V. Cerundolo, H. Allen, and A. Townsend. 1992. Structural requirements for the peptide-induced conformational change of free major histocompatibility complex class I heavy chains. *Eur. J. Immunol.* 22: 2085–2091.
76. Lilić, M., Z. Popmihajlov, J. J. Monaco, and S. Vukmanović. 2004. Association of β_2-microglobulin with the α_3 domain of H-2D^b heavy chain. *Immunogenetics* 55: 740–747.
77. Rammensee, H. G., T. Friede, and S. Stevanoviíc. 1995. MHC ligands and peptide motifs: first listing. *Immunogenetics* 41: 178–228.
78. Theodossis, A., C. Guillonneau, A. Welland, L. K. Ely, C. S. Clements, N. A. Williamson, A. I. Webb, J. A. Wilce, R. J. Mulder, M. A. Dunstone, et al. 2010. Constraints within major histocompatibility complex class I restricted peptides: presentation and consequences for T-cell recognition. *Proc. Natl. Acad. Sci. USA* 107: 5534–5539.
79. Wallny, H. J., D. Avila, L. G. Hunt, T. J. Powell, P. Riegert, J. Salomonsen, K. Skjødt, O. Vainio, F. Vilbois, M. V. Wiles, and J. Kaufman. 2006. Peptide motifs of the single dominantly expressed class I molecule explain the striking MHC-determined response to Rous sarcoma virus in chickens. *Proc. Natl. Acad. Sci. USA* 103: 1434–1439.
80. Di Marco, M., H. Schuster, L. Backert, M. Ghosh, H. G. Rammensee, and S. Stevanović. 2017. Unveiling the peptide motifs of HLA-C and HLA-G from naturally presented peptides and generation of binding prediction matrices. *J. Immunol.* 199: 2639–2651.
81. Guillaume, P., S. Picaud, P. Baumgaertner, N. Montandon, J. Schmidt, D. E. Speiser, G. Coukos, M. Bassani-Sternberg, P. Filippakopoulos, and D. Gfeller. 2018. The C-terminal extension landscape of naturally presented HLA-I ligands. *Proc. Natl. Acad. Sci. USA* 115: 5083–5088.

82. Gakamsky, D. M., P. J. Bjorkman, and I. Pecht. 1996. Peptide interaction with a class I major histocompatibility complex-encoded molecule: allosteric control of the ternary complex stability. *Biochemistry* 35: 14841–14848.
83. Gakamsky, D. M., L. F. Boyd, D. H. Margulies, D. M. Davis, J. L. Strominger, and I. Pecht. 1999. An allosteric mechanism controls antigen presentation by the H-2K^b complex. *Biochemistry* 38: 12165–12173.
84. Blees, A., D. Januliene, T. Hofmann, N. Koller, C. Schmidt, S. Trowitzsch, A. Moeller, and R. Tampé. 2017. Structure of the human MHC-I peptide-loading complex. *Nature* 551: 525–528.
85. Jiang, J., K. Natarajan, L. F. Boyd, G. I. Morozov, M. G. Mage, and D. H. Margulies. 2017. Crystal structure of a TAPBPR-MHC I complex reveals the mechanism of peptide editing in antigen presentation. *Science* 358: 1064–1068.
86. Thomas, C., and R. Tampé. 2017. Structure of the TAPBPR-MHC I complex defines the mechanism of peptide loading and editing. *Science* 358: 1060–1064.
87. McShan, A. C., K. Natarajan, V. K. Kumirov, D. Flores-Solis, J. Jiang, M. Badstübner, J. S. Toor, C. R. Bagshaw, E. L. Kovrigin, D. H. Margulies, and N. G. Sgourakis. 2018. Peptide exchange on MHC-I by TAPBPR is driven by a negative allostery release cycle. *Nat. Chem. Biol.* 14: 811–820.
88. Pedersen, L. O., A. Stryhn, T. L. Holter, M. Etzerodt, J. Gerwien, M. H. Nissen, H. C. Thøgersen, and S. Buus. 1995. The interaction of beta 2-microglobulin (β_2m) with mouse class I major histocompatibility antigens and its ability to support peptide binding. A comparison of human and mouse β_2m. *Eur. J. Immunol.* 25: 1609–1616.
89. Paquet, M. E., and D. B. Williams. 2002. Mutant MHC class I molecules define interactions between components of the peptide-loading complex. *Int. Immunol.* 14: 347–358.
90. Sagert, L., F. Hennig, C. Thomas, and R. Tampé. 2020. A loop structure allows TAPBPR to exert its dual function as MHC I chaperone and peptide editor. *eLife* 9: e55326.
91. Pérarnau, B., C. A. Siegrist, A. Gillet, C. Vincent, S. Kimura, and F. A. Lemonnier. 1990. β_2-microglobulin restriction of antigen presentation. *Nature* 346: 751–754.
92. Rammensee, H. G., P. J. Robinson, A. Crisanti, and M. J. Bevan. 1986. Restricted recognition of β_2-microglobulin by cytotoxic T lymphocytes. *Nature* 319: 502–504.